Simulating feldspar luminescence phenomena using R

Pagonis, Vasilis; Schmidt, Christoph; Kreutzer, Sebastian

Published in:
Journal of Luminescence

DOI:
10.1016/j.jlumin.2021.117999

Publication date:
2021

Citation for published version (APA):
Pagonis, V., Schmidt, C., & Kreutzer, S. (2021). Simulating feldspar luminescence phenomena using R. *Journal of Luminescence*, *235*, [117999]. https://doi.org/10.1016/j.jlumin.2021.117999

Simulating feldspar luminescence phenomena using R

Vasilis Pagonis[a,*], Christoph Schmidt[b], Sebastian Kreutzer[c,d]

[a] *McDaniel College, Physics Department, Westminster, MD 21157, USA*
[b] *University of Lausanne, Institute of Earth Surface Dynamics, Géopolis, Lausanne, Switzerland*
[c] *Geography & Earth Sciences, Aberystwyth University, Wales, United Kingdom*
[d] *IRAMAT-CRP2A, Université Bordeaux Montaigne, France*

Abstract

Kinetic models have been used extensively for modeling and numerical simulation of luminescence phenomena and dating techniques, for various dosimetric materials. Several comprehensive models have been implemented for quartz, which allow simulation of complex sequences of irradiation and thermal/optical events in nature and in the laboratory. In this paper we present a simple and accurate way of simulating similarly complex sequences in feldspars. We introduce the open-access R scripts Feldspar Simulation Functions (FSF), for kinetic model simulation of luminescence phenomena in feldspars. These R functions offer useful numerical tools to perform luminescence simulations in a user-friendly manner. The mathematical framework of four different types of previously published models is presented in a uniform way, and the models are simulated with FSF. While previously published versions of these four models require numerical integration of the differential equations, FSF circumvent the need for numerical integration by using accurate summations over the finite range of the model parameters. The simulation process can be understood easily by creating transparent sequences of events, consisting of these compact R functions. The key physical concept of the FSF is that irradiation and thermal/optical treatments of feldspars change the distribution of nearest neighbor (NN) distances in donor-acceptor pairs. These changes are described using analytical equations within the four models examined in this paper. The NN distribution at the end of one simulation stage becomes the initial distribution for the next stage in the sequences of events being simulated. Several practical examples and possible applications and extensions of the FSF are discussed.

Keywords: Luminescence, Feldspar, Tunneling, R, Optically Stimulated Luminescence, Infrared Stimulated Luminescence, Thermoluminescence, Thermochronometry

*Corresponding author
Email address: vpagonis@mcdaniel.edu (Vasilis Pagonis)

1. Introduction

Phenomenological models are frequently used to describe experimental signals in stimulated luminescence experiments. Within these phenomenological models, various experimental stimulation methods are commonly used in the laboratory. Specifically thermal stimulation produces thermoluminescence (TL) signals , while optical stimulation with visible or infrared light produces optically or infrared stimulated luminescence (OSL, IRSL). For a review of the models commonly used to describe these signals, the readers are referred to available textbooks (e.g., Chen and Pagonis, [1], Yukihara and McKeever [2]), and the recent review article by Kitis et al. [3].

Typically, phenomenological luminescence models consist of systems of differential equations describing various electronic transitions. In most cases, these equations must be solved numerically using appropriate initial conditions, while analytical solutions have been developed for some of the simpler models. These phenomenological models have been used extensively to simulate, for example, the complex histories of geological quartz samples, as well as the complex experimental luminescence protocols used routinely for quartz samples in the laboratory (Bailey [4], Pagonis et al. [5], Friedrich et al. [6]).

While several simulations of complex sequences of irradiation and optical/thermal treatments have been implemented for quartz, there exist very few such comprehensive studies of complex sequences for feldspars (Polymeris et al. [7], Pagonis et al. [8], Brown et al. [9]).

The overall purpose of this paper is to demonstrate how researchers can simulate complex sequences of irradiation and thermal/optical events in feldspars, by using a simple and accurate method which does not require numerical integrations.

This article contains the following accomplishments:

- Four previously published general luminescence models involving quantum tunneling phenomena are summarized, and their mathematical formalism is presented. Even though the models discussed here do not contain new modeling concepts, the purpose of this paper is to pool existing models on feldspar luminescence production transparently, and to develop open-source software which can be shared and further developed in the future by the luminescence dosimetry community.

- The chosen models in this paper are based on first order kinetics, and *partial* analytical solutions are available in the literature for three of them. We present a new partial analytical solution for the fourth model.

- By using these partial analytical solutions, we detail flexible short R scripts [10], which do not require numerical integration of the differential equations.

- We show how the R functions can be combined to simulate complex sequences of irradiation, heating and optical excitation of feldspar samples.

The overall organization of this paper is as follows:

Section 2 introduces quantum tunneling and the distribution of nearest neighbors in a random distribution of defects, and is followed in section 3 by a general discussion of published luminescence models involving quantum tunneling phenomena. Section 4 presents the four first order kinetics models studied in this paper, and is followed in sections 5 and 6 by two models based on quantum tunneling taking place from the ground state of the electron trap.

Section 7 presents the R codes for processes involving the excited state of the trapped electrons, and is followed by simulations of continuous wave IRSL (CW-IRSL) and TL signals from freshly irradiated samples (sections 8 and 9).

Section 10 presents several examples of how the R functions can be combined to simulate a variety of multiple stage experiments, involving thermal and/or optical treatments of samples in the laboratory. Section 11 presents R code for a recent model, which was developed for low temperature thermochronometry. Finally, section 12 presents least squares fitting scripts, which can be used to analyze experimental TL and CW-IRSL data from freshly irradiated samples.

The paper ends with a discussion containing suggestions for possible applications of the FSF in luminescence research.

2. Quantum tunneling and the distribution of nearest neighbors in a random distribution of defects

During the past decade significant progress has been made both experimentally and theoretically in understanding the behavior of luminescence signals from feldspars, apatites and other natural materials. Quantum mechanical tunneling and the associated phenomenon of "anomalous fading" of these luminescence signals are now well established as dominant mechanisms in these materials (for a recent overview see for example Pagonis et al. [11]).

From a modeling point of view, one considers a random distribution of electrons and positive charges in a crystal, and introduces the concept of the distribution of nearest neighbor distances. The positive charges in this random distribution can be ions, or holes, and will be referred to with the general term of acceptors.

Two of the common assumptions of quantum tunneling models based on random distributions of electrons and positive ions are: (a) An electron tunnels from a donor to the nearest acceptor, and (b) the concentration of electrons is much lower than that of acceptors

at all times during the tunneling process. Because of this latter assumption, the acceptor concentration ρ (m^{-3}) of positive ions will remain practically constant during the tunneling process, and ρ can be used to characterize the system.

The quantum tunneling process takes place in this random distribution, and the probability per unit time that a trapped electron will tunnel to a positive charge is given by the exponential decay behavior of the wavefunction (Tachiya and Mozumder [12]):

$$P(r) = s \exp(-r/a) \tag{1}$$

where s (s^{-1}) is the frequency parameter characterizing the tunneling process, r (m) is the actual donor-acceptor distance, and the length a (m) represents the attenuation length of the ground state wavefunction. The inverse of the tunneling length a is called the potential barrier penetration constant $\alpha = 1/a$ (m^{-1}).

One introduces now two dimensionless quantities r' and ρ', instead of r and ρ. First, a distance parameter r' is defined by:

$$r' = (4\pi\rho/3)^{1/3} r \tag{2}$$

where ρ (m^{-3}) represents the density of acceptors in the material per unit volume. Notice that r' is directly proportional to the actual distance r, simply scaled by a factor $(4\pi\rho/3)^{1/3}$ which depends on the acceptor density ρ. Secondly, one also introduces a dimensionless acceptor density parameter ρ' by:

$$\rho' = (4\pi\rho/3) a^3 \tag{3}$$

where the tunneling length a (m) was defined above. Notice that ρ' is directly proportional to the acceptor density ρ, simply scaled by a "unit tunneling volume" $4\pi a^3/3$.

As a concrete example, let us consider a cube with side $d = 100$ nm, containing 50 electrons and 300 recombination centers (acceptors), as shown in Fig.1(a). The tunneling distance is $a = 0.11$ nm and the tunneling parameter $\alpha = 1/a = 9 \times 10^9$ m^{-1}. The density of acceptors in this cube is $\rho = 300/d^3 = 3 \times 10^{23}$ m^{-3}. The dimensionless acceptor density is then $\rho' = (4\pi\rho/3) a^3 = 1.67 \times 10^{-6}$.

For random distributions of defects, the distribution of nearest neighbors is given by the Poisson probability of finding no neighbors in a sphere of radius r (see for example Jain et al. [13]):

$$g(r) = 4\pi\rho r^2 \exp\left[-4\pi\rho/3 (r)^3\right] \tag{4}$$

By using the dimensionless length r' and dimensionless acceptor density ρ', this distribution function becomes:

$$g(r') = 3\,(r')^2\,\exp\left[-\,(r')^3\right] \tag{5}$$

It must be noted that the distribution $g(r')$ in Eq.(5) is a purely geometrical concept, and there is no specific physical process associated with it. The physics of the system is contained in the tunneling length a, and will be considered in later sections. It is also noted that in some published models, the symbol $p(r')$ is used instead of $g(r')$.

Eq.(5) is usually referred to as the *unfaded* distribution of distances.

Fig.1 depicts the nearest neighbor distribution of distances $g(r')$ between electrons and acceptors in the cube discussed above. The R code used to produce Fig.1 evaluates the nearest neighbor distribution of distances between electrons and acceptors in the cube. The R package *plot3D* [14] is used to plot the random locations of the electrons (triangles) and acceptors (circles). The R package *FNN* [15] is used to evaluate the nearest-neighbor distance between each pair of electron and positive charge, and the code produces a histogram of the distribution of nearest neighbor distances in the system.

All models considered in this paper are described mathematically by the concentration $n(r', t)$ of trapped electrons, which is a function of the distance r' and of the elapsed time t. Let us denote the total concentration of traps in the material by N, and further assume that at time $t = 0$ all N traps are filled. With this assumption, the distribution of trapped electrons $n(r', 0)$ at different distances r' and at time $t = 0$, is given by:

$$n(r', 0) = Ng(r') = 3N\,(r')^2\,\exp\left[-\,(r')^3\right] \tag{6}$$

At any later time t, the concentration $n(r', t)$ of trapped electrons varies with both the distance parameter r' and with the elapsed time t, due to various physical processes taking place in the crystal, e.g., irradiation processes, thermal and/or optical treatments of the sample etc.

The specific goal of this paper is to develop general R functions, which can simulate the history of feldspar samples during geological times and also in laboratory experiments.

The time evolution of the distribution of distances $n(r', t)$ is the key for the development of these functions. One can simply use the *final* distribution of distances $n\,(r', t)$ at the end of each stage in the simulations, as the *initial* distribution of distances for the next stage in the simulations. The second key to the development of the FSF is the availability of analytical equations for $n\,(r', t)$ when the distance r' is considered a constant. These analytical equations are available for each of the four models studied for this paper, and are discussed in the next section.

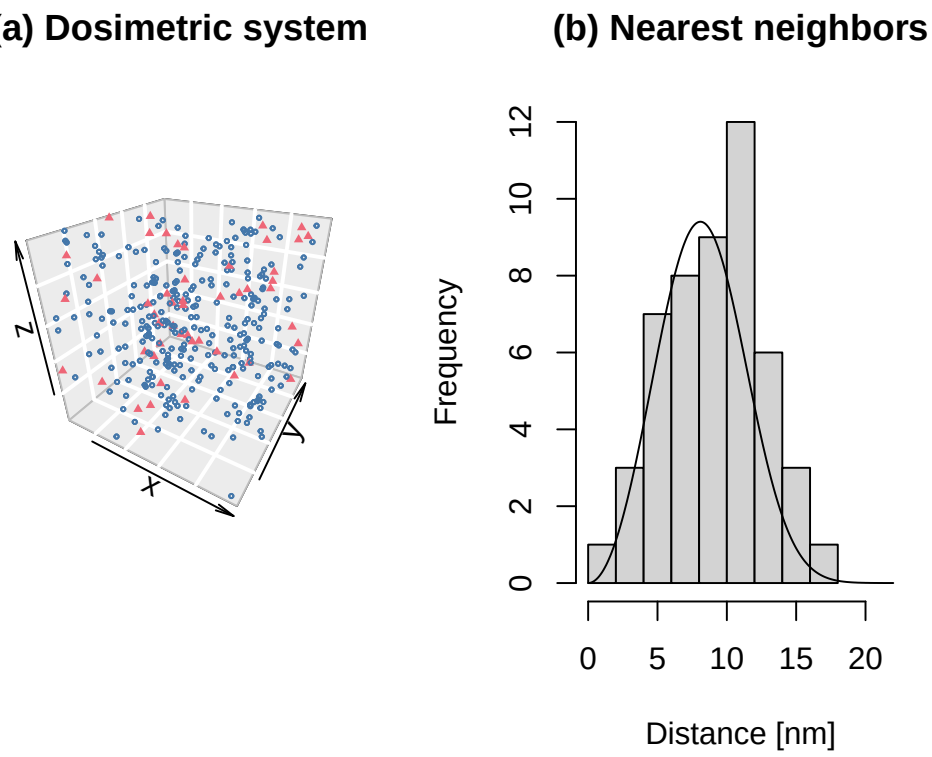

Figure 1: (a) A cube with side $d = 100$ nm contains 50 electrons (triangles) and 300 acceptors (circles). (b) Histogram of the actual nearest neighbor distances (in nm) of electron-acceptor pairs from the cube in (a). The solid line represents the analytical equation for the distribution of nearest neighbors Eq.(4). For more details, see Pagonis and Kulp [16].

3. Overview of models based on quantum tunneling transitions

Several types of models have been investigated in the literature, in order to explain the luminescence signals in feldspars, based on quantum tunneling transitions. In general, these models fall into two broad categories: first order kinetics models (FOK), and general order kinetics models (GOK).

In this paper we will consider four models based on first order kinetics, which are shown schematically in Fig.2. Previously studied GOK models from the bibliography are considered in the Discussion section of this paper.

These four FOK models were chosen for the following reasons:

1. *Partial* analytical equations for three of the four FOK models are already available in the literature. A new partial analytical solution is presented in this paper for the fourth model.

2. These partial analytical equations enabled the development of simple and fast FSF, by

replacing a *double* numerical integration with a *single* finite sum, as will be explained in the rest of this section.

3. The four models build on each other, and become progressively more complex. However, the structure of the FSF code remains the same for all four models, thus providing a template for extending the FSF to more complex models, such as the band tail states model of feldspars (e.g., King et al. [17], Li and Li [18], Jain and Ankjærgaard [19], Poolton et al. [20]).

The goal of either FOK or GOK models is to evaluate the total concentration $n(t)$ of trapped electrons at time t. Mathematically, one has to carry out a double numerical integration over the elapsed time t, and over the distance parameter r':

$$n\left(t\right) = \int_0^{t'} \int_0^{\infty} \frac{\partial n\left(r', t\right)}{\partial t} dr'\, dt' \tag{7}$$

However, as will be described in the next few sections, in FOK models the double integration in Eq.(7) can be replaced by a single integration over r':

$$n\left(t\right) = \int_0^{\infty} F(r') dr' \tag{8}$$

where $F(r')$ is an analytical function which depends on the distance parameter r'. Further simplification of the R codes is achieved by replacing the integration over r' in Eq.(8) with a summation over the finite range of this parameter. This summation procedure is discussed in section 5.

4. The four first order kinetics feldspar models

The first type of quantum mechanical tunneling is considered to take place directly from the ground state of the trap, as shown in Fig.2a. For the purposes of this paper, we will refer to this type of model as ground state tunneling (GST) model, and initially it was developed by Tachiya and Mozumder [12]) within the context of the kinetics of chemical reactions. Several decades later this model was shown to be associated with a power-law type of decay of the luminescence signal (Huntley [21]).

Huntley and Lian [22] suggested an extension of the GST model in the Appendix of their paper, and this model is shown schematically in Fig.2b. This model uses a first order differential equation to describe simultaneous natural irradiation and anomalous fading effects on the luminescence of feldspars, and was examined in detail in the papers by Li and Li [23],

Kars et al. [24] and Kars and Wallinga [25]. We will refer to this model as an irradiation ground state tunneling (IGST) model. Kars et al. [25] applied the model of Huntley and Lian [22] to construct unfaded and natural dose response curves (DRCs) of IRSL signals.

The second type of quantum mechanical tunneling is considered to take place via the excited state of the trap, as shown in Fig.2c. Historically, this type of model was first considered by Thioulouse et al. [26], and Chang and Thioulouse [27]. Almost 30 years later, Jain et al. [13] developed further this kinetic model, which quantifies localized recombination within randomly distributed donor-acceptor pairs. We will refer to this type of model as an excited state tunneling (EST) model.

The fourth type of model was developed recently by Brown et al. [9] for the purposes of low temperature thermochronometry (King et al. [28]), and is shown schematically in Fig.2d. These authors extended the original model by Jain et al. [13] to include irradiation processes. This model also uses a first order differential equation to describe simultaneous irradiation, quantum tunneling and thermal excitation effects. We will refer to this model as a thermally assisted excited state tunneling (TA-EST) model.

In the rest of this paper we will summarize the mathematical description of these four models, point out their similarities and differences, and will develop appropriate R functions to simulate a wide variety of electronic processes in feldspars.

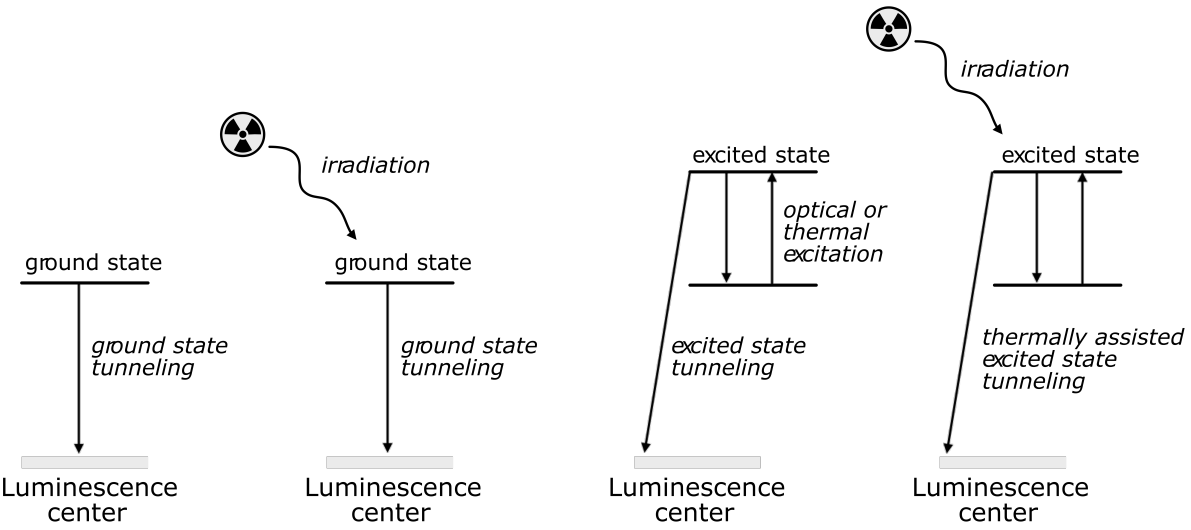

Figure 2: Schematic depiction of the four models in this paper: (a) The ground state tunneling (GST) model (Tachiya and Mozumder [12], Huntley [21]). (b) The more general irradiation and ground state tunneling (IGST) model, in which anomalous fading and natural irradiation are taking place simultaneously (Huntley and Lian [22]). (c) The excited state tunneling (EST) model (Jain et al. [13]) (d) Simultaneous irradiation and thermally assisted excited state tunneling (TA-EST) model by Brown et al. [9].

Table 1 shows the various FSF and summarizes their purpose. We will discuss each one of these functions in subsequent sections. A detailed listing of the FSF, as well as instructions for loading the code is available open-access at http://doi.org/10.5281/zenodo.4429270 (Pagonis et al. [29]).

5. Ground state tunneling: the anomalous fading effect

Extensive experimental and modeling studies revealed a time dependent localized tunneling/recombination probability in a variety of dosimetric materials. Of major interest is the "anomalous fading" of luminescence signals observed mainly in feldspars and apatites (Lamothe et al. [30], and references therein). These studies have provided very strong evidence that the anomalous fading effect is due to quantum mechanical tunneling from the ground state of the trap to the luminescence center (Visocekas et al. [31], [32]).

In the GST model of Fig.2a, the tunneling mechanism takes place in a random distribution of acceptors and electrons in the crystal, and transitions take place directly from the ground state of the system. In this model, the distribution of electrons in the ground state $n(r', t)$ varies both with the distance parameter r' and with the elapsed time t , according to the

Table 1: The various FSF developed in this paper.

THE FELDSPAR SIMULATION FUNCTIONS	**Model**
AFfortimeT(time, rprimes, rho, s) Evaluates nearest neighbor distribution at the end of the anomalous fading period. This function is based on Eq.(10).	GST
irradfortimeT(tirr, rprimes, rho, s, Ddot, D0) Evaluates nearest neighbor distribution at the end of the irradiation time. This function is based on Eq.(18).	IGST
CWfortimeT (timCW, rho, rprimes, A)) Evaluates nearest neighbor distribution at the end of the IR stimulation period. This function is based on Eq.(29).	EST
CWsignal (timCW, rho, rprimes, A, distr = NULL) Evaluates and returns the partial CW-IRSL signals for each distance r'.	EST
stimIRSL (...) Evaluates and returns the total CW-IRSL signal.	EST
heatTo(Tph, E, s, beta, rho, rprimes, distr = NULL) Evaluates nearest neighbor distribution at the end of preheating to temperature T_{ph} (in °C). This function is based on Eq.(34).	EST
heatAt(Tph, tph, E, s, rprimes, distr = NULL) Evaluates nearest neighbor distribution at the end of preheating for time t_{ph} (in s) and at a temperature T_{ph} (in °C).	EST
TLsignal(temp, E, s, rho, rprimes, distr = NULL) Evaluates and returns the partial TL signals for each distance r'.	EST
stimTL (...) Evaluates and returns the total TL signal.	EST
irradandThermalfortimeT(Tirr,tirr,E,s,rho,rprimes,D0,Ddot,distr= NULL) Evaluates nearest neighbor distribution for various irradiation time t_{irr} (in s), for a fixed sample temperature T_{irr} (in °C).	TA-EST
irradatsometemp(Tirr,tirr,E,s,rho,rprimes,D0,Ddot, distr = NULL) Evaluates nearest neighbor distribution for various sample temperatures T_{irr} (in °C), for a fixed irradiation time t_{irr} (in s).	TA-EST

differential equation:

$$\frac{\partial n\left(r',t\right)}{\partial t} = -n\left(r',t\right) s \exp\left[-\left(\rho'\right)^{-1/3} r'\right] \tag{9}$$

We assume that at time $t = 0$ the distribution of distances is given by the nearest neighbor distribution $g(r') = 3\left(r'\right)^2 \exp\left[-\left(r'\right)^3\right]$, shown in Eq.(5).

The analytical solution of this first order differential equation for a constant distance parameter r' is the simple exponential function:

$$n\left(r',t\right) = N\, 3\left(r'\right)^2 \exp\left[-\left(r'\right)^3\right] \exp\left[-s\, t\, \exp\left[-\left(\rho'\right)^{-1/3} r'\right]\right] \tag{10}$$

where N is the total concentration of traps in the material. The value of N is a scaling factor in all four models discussed in this paper, and we are mostly interested in the trap filling ratio $n(t)/N$, instead of the actual value of N.

The total concentration of trapped electrons at time t is evaluated numerically by integrating $n\left(r',t\right)$ over all possible values of the variable r' (see Huntley [21]):

$$n\left(t\right) = \int_0^\infty n\left(r',t\right) dr' = N \int_0^\infty g(r') \exp\left\{-s \exp\left[-\left(\rho'\right)^{-1/3} r'\right] t\right\} dr' \tag{11}$$

$$n\left(t\right) = \int_0^\infty n\left(r',t\right) dr' = N \int_0^\infty g(r') \exp\left\{-s_{eff}(r')\, t\right\} dr' \tag{12}$$

where we have defined an effective frequency factor $s_{eff}(r')$ by:

$$s_{eff}(r') = s \exp\left[-\left(\rho'\right)^{-1/3} r'\right] \tag{13}$$

Equation (12) can be interpreted as the sum of several decaying exponential functions $A \exp\left(-\lambda t\right)$, with each of these exponentials having a different amplitude given by $g(r')$ and a different effective decay constant $\lambda = s_{eff}(r')$. In the code which follows, we will calculate the integral in Eq.(11) and in other similar equations, by using a *summation* over the different r' values, instead of a formal integration. For all practical purposes, the summation can be carried out up to a maximum distance parameter $r' = 2.2$, which is the upper limit of the extent of the function $g(r')$. For an implementation of this method using a Monte Carlo method, see the detailed study by Pagonis et al. [33]. In this method, one is then evaluating the function $n(t)$ in Eq.(12) by adding several exponential functions, thus:

$$n(t) = N \sum_{r'=0}^{r'=2.2} 3\left(r'\right)^2 \exp\left[-\left(r'\right)^3\right] \exp\left[-s_{eff}\left(r'\right)\, t\right] \Delta r' \tag{14}$$

The parameter $\Delta r'$ is an appropriate small interval, with a typical small value of $\Delta r'$=0.01. The summation indicated in Eq.(14) was compared with the more accurate numerical integration shown in Eq.(12), and the numerical results from the two approaches agreed to better than 1%.

The first FSF from Table 1 is ***AFfortimeT()***, and a simulation of the anomalous fading effect is shown in Listing 1, with a typical output shown in Fig.3. For simplicity and clarity, Listing 1 contains a minimal R script required to produce the results of Fig.3, and the actual script contains additional graphics commands not shown in Listing 1. The complete scripts which produce the figures in this paper can be found in the GitHub repository referenced through Zenodo, http://doi.org/10.5281/zenodo.4429270.

Line 1 loads the R-code for the FSF using the ***source()*** command. Lines 2 and 3 in this short code define the values of s and ρ', while line 4 defines the fading times for the simulation as the parameter ***timesAF*** $= 0, 10^2, 10^4, 10^6$ a after the start of the tunneling process. The value of ***timesAF***$= 0$ corresponds to the nearly symmetric unfaded distribution of distances r'. Line 5 defines a vector ***rprimes*** corresponding to values of r' from $r' = 0$ to a maximum of $r' = 2.2$, in steps of $dr' = 0.002$. This line of code also defines how many exponentials we are adding in order to calculate $n(t)$. For example, in the case of $r' = 0$ to $r' = 2.2$ in steps of $\Delta r' = 0.002$, we are adding a total of 1,100 exponential curves.

Line 6 calls the function ***AFfortimeT()*** which calculates the concentration $n(r', t)$ indicated in Eq.(10); the R function ***sapply()*** is used in the same line to carry out the evaluation for all four fading times. By default, the function ***AFfortimeT()*** uses the initial unfaded distribution of distances at time $t = 0$, given in Eq.(5).

The matrix ***distribs*** in line 6 contains four columns, corresponding to the four fading times. This simplifies and speeds up significantly the calculation of the total remaining charge $n(t)$ in Eq.(14). Finally ***matplot()*** is used in line 7 to plot the four distributions of r' at the fading times $times = 0, 10^2, 10^4, 10^6$ a.

```
source("Functions_FSFpaper.R")                    # Load the FSF R-codes
s <- 3e15                                         # frequency factor
rho <- 1e-6                                       # rho' value
timesAF <- 3.154e7 * c(0, 1e2, 1e4, 1e6)          # fading times 0-10^6 a
rprimes <- seq(from = 0, to = 2.2, by = 0.002)    # r' = 0-2.2
distribs <- sapply(timesAF, AFfortimeT, rprimes, rho, s)
matplot(rprimes, distribs)

n <- 0.002 * colSums(distribs)
plot(timesAF / (3600 * 24), 100 * n)
```

LISTING 1

R code demonstrating the function ***AFfortimeT()*** in a simulation of the charge distributions $n(r', t)$ within the GST model shown in Fig.2a.

Figure 3 shows an example of the distribution obtained using Eq.(10) as a function of the dimensionless distance r', and at times $t = 0, 10^2, 10^4, 10^6$ a after the start of the tunneling process. The solid line indicates the initial unfaded peak-shaped symmetric distribution at time $t = 0$. The values of the parameters used in Fig.3 are typical for ground state tunneling in feldspars, $\rho' = 1 \times 10^{-6}$ and $s = 3 \times 10^{15}$ s^{-1}. The sharply rising dashed lines in Fig.3 represent the "moving tunneling fronts" in the tunneling process. The characteristic shape of this tunneling front is the product of the two functions appearing in Eq.(10), namely of the sharply rising double-exponential function $\exp\left[-s\,t\,\exp\left[-\left(\rho'\right)^{-1/3} r'\right]\right]$ and of the symmetric nearest neighbor distribution $3\left(r'\right)^2 \exp\left[-\left(r'\right)^3\right]$ (see for example, the detailed discussion in Pagonis and Kitis [34]).

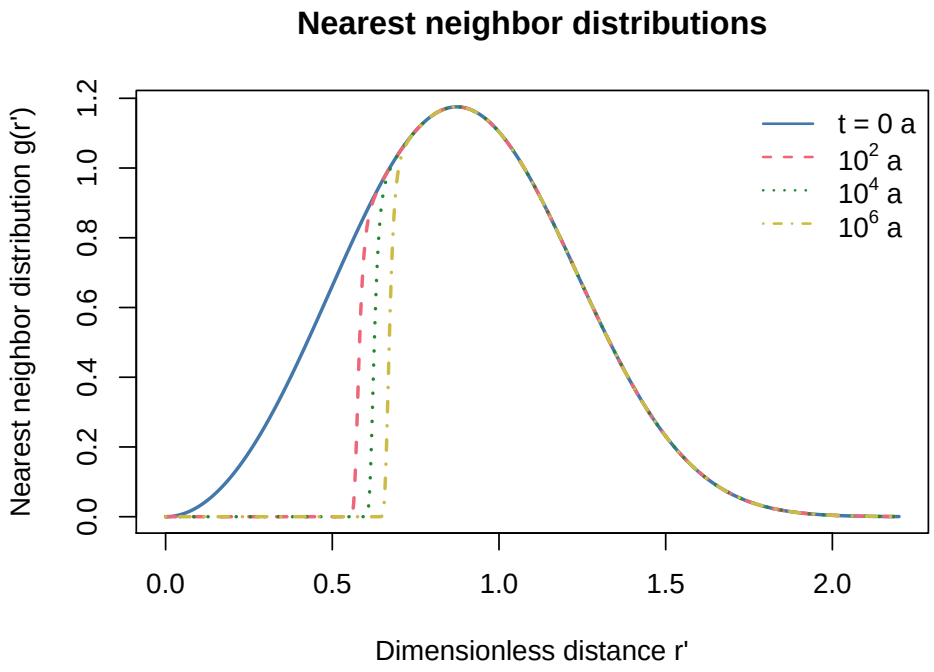

Figure 3: Examples of using the FSF *AFfortimeT()*, to evaluate the nearest neighbor distribution at different times $t = 0, 10^2, 10^4, 10^6$ a. The solid line represents the *unfaded* nearly symmetric distribution at time $t = 0$. The "tunneling front" is the almost vertical line which moves to the right as more and more electrons are recombining at larger distances r' (for more details, see for example Li and Li [23]).

We can describe the AF process both in nature over a long geological period, as well as in the laboratory over a much shorter time period, by evaluating the total concentration $n(t)$, as shown in the short code of Listing 2. The only change necessary in order to simulate geological or laboratory time scales is to change the argument *timesAF* of the function, from a geological time period 0-10^6 a, to a laboratory time of 0-10 days.

Only two extra lines 9 and 10 of code are needed in Listing 1 in order to produce the plot of $n(t)$ in the GST model, as follows:

Line 9 calculates the sum over all distances r' indicated in Eq.(14), by using *colSums()* to add the columns of the matrix *distribs* created in line 5. The result of *colSums()* is multiplied by the distance interval $\Delta r' = 0.002$, as defined in line 4 of the code by the parameter *rprimes*. Finally, line 10 plots the remaining charge $n(t)$ as a function of the fading time. The result of the code is shown in Fig.4a; after 10^4 a, approximately 78% of the trapped electrons remain in the sample, and 74% remain after 10^6 a. The time scale in Fig.4a is plotted only up to 10^4 a, in order to show clearly the sharp initial drop in the remaining charge $n(t)$. The values of the parameters used in Fig.4ab are the same as in Fig.3.

Fig.4b simulates the AF process after 10 days in the laboratory, with approximately 87% of the trapped electrons remaining in the sample. If desired, the user can add a few more lines of code, in order to obtain the g-value characterizing the AF process (see for example Pagonis and Kitis [34]).

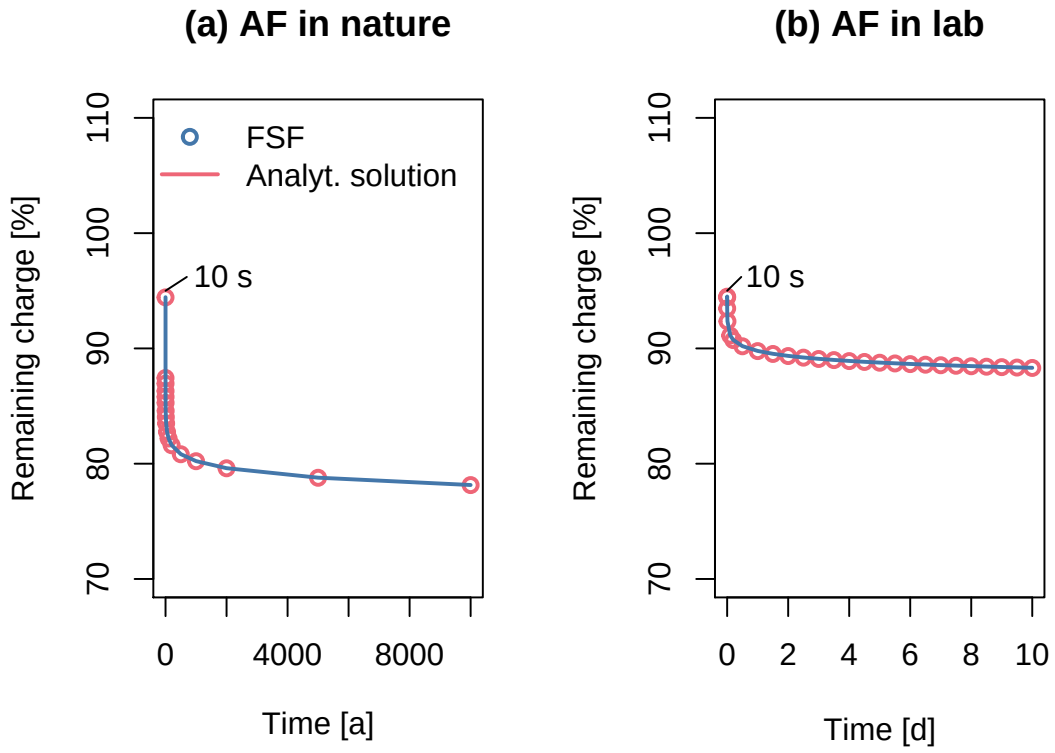

Figure 4: (a) Simulation of long term anomalous fading in nature over a time period of 10^4 years, starting with an unfaded sample and using the FSF `AFfortimeT()`. The solid line indicates the approximate analytical Eq.(16). (b) Short term AF in the laboratory, over a period of 10 days after the end of irradiation. The parameters in the model are typical for feldspars. For more examples, see Li and Li [23].

We can compare the results of these simulations with the semi-analytical version of the model described in Huntley [21]. In this approximation, one introduces a critical tunneling lifetime τ_c and a corresponding critical radius r'_c , which describes the behavior of the physical system. From a physical point of view, τ_c can be understood as the tunneling lifetime of those remaining pairs that are separated by the critical tunneling distance r'_c (Jain et al. [13]). Geometrically, this approximation corresponds to replacing the dashed lines in Fig.3 by a vertical line. Mathematically the value of the critical distance is given by (Pagonis and Kitis [34]):

$$r'_c = (\rho')^{1/3} \ln(zs\,t) \tag{15}$$

where $z = 1.8$ is a correction factor which was introduced arbitrarily by Huntley [21], but was explained mathematically later by Pagonis and Kitis [34]. In the example of Fig.3 we

see that after 100 years, the almost vertical line representing the tunneling front, has moved to a critical radius $r'_c \simeq 0.6$. We can verify this value of r'_c, by substituting the values of the parameters in Eq.(15):

$$r'_c = (\rho')^{1/3} \ln(zs\,t) = \left(10^{-6}\right)^{1/3} \ln\left[1.8(3\times10^{15})\ \left(100\times3.154\times10^{7}\right)\right] = 0.58$$

in agreement with Fig.3. In this approximate model of ground state tunneling, the following analytical equation expresses the concentration of charge carriers in the ground state $n(t)$ during geological time scales:

$$n(t) = n_0 \exp\left(-\rho'\ \ln\left[z\ s\ t\right]^3\right) \tag{16}$$

A plot of this equation is shown by the solid lines in Fig.4ab. The analytical expression for the remaining charge $n(t)$ in Eq.(16) agrees well with the result of the FSF (Pagonis and Kitis [34]).

Next we develop the FSF for the IGST model shown in Fig.2b.

6. Simultaneous irradiation and quantum tunneling

In this section we develop an R function for the IGST model shown in Fig.2b. The model is based on the differential equation of Huntley and Lian [22], and has been studied by Li and Li [23], as well as by Kars and Wallinga [25]. These authors and carried out an extensive experimental and modeling study of both laboratory-irradiated and naturally irradiated feldspars.

Li and Li [23] investigated the simultaneous effects of irradiation and tunneling by using the differential equation:

$$\frac{\partial n(r',t)}{\partial t} = \frac{\dot{D}}{D_0}\left[N(r') - n(r',t)\right] - n(r',t)\, s \exp\left[-(\rho')^{-1/3} r'\right] \tag{17}$$

where s (s^{-1}) is the frequency characterizing the ground state tunneling process, $\dot{D}$ (Gy s^{-1}) is the dose rate, and D_0 (Gy) is the characteristic dose of the sample. This equation is valid for samples irradiated in nature with a very low dose rate $\dot{D}$ of the order of 10^{-11} (Gy s^{-1}), but also for samples irradiated with much higher dose rates of about 0.1 (Gy s^{-1}) used in the laboratory. The parameter $N(r') = N\, g(r')$ represents the total concentration of traps corresponding to a distance parameter r', and N is the total number of traps in the sample. The rest of the parameters in this equation have the same meaning as in the previous section.

The first term in Eq.(17) represents the rate of increase of the concentration of trapped electrons due to irradiation, while the second term represents the decrease in the concentration due to the effect of ground state tunneling, as previously. The solution of the first order differential Eq.(17) when one starts with initially empty traps concentration $n\left(r',0\right)=0$, is the following simple saturating exponential function (Li and Li [23]):

$$n\left(r',t\right)=N\,g\left(r'\right)\frac{\dot{D}}{D_0 s_{eff}\left(r'\right)+\dot{D}}\left[1-\exp\left\{-\left[\frac{\dot{D}}{D_0}+s_{eff}\left(r'\right)\right]t\right\}\right] \tag{18}$$

where we defined the effective frequency $s_{eff}\left(r'\right)$ for the process as:

$$s_{eff}\left(r'\right)=s\exp\left[-\left(\rho'\right)^{-1/3}r'\right] \tag{19}$$

The total concentration of trapped electrons at time t is evaluated numerically by integrating $n\left(r',t\right)$ over all possible values of the variable r':

$$n\left(t\right)=\int_0^\infty n\left(r',t\right)dr' \tag{20}$$

$$n\left(t\right)=\int_0^\infty Ng(r')\frac{\dot{D}}{D_0 s_{eff}\left(r'\right)+\dot{D}}\left[1-\exp\left\{-\left[\frac{\dot{D}}{D_0}+s_{eff}\left(r'\right)\right]t\right\}\right]dr' \tag{21}$$

The modeling results of Li and Li [23] were expressed in terms of integral equations, which require numerical integration over the distances r' in the model. As mentioned in the previous section, the R functions developed in this paper circumvent the need for these numerical integrations, by replacing them with finite sums over the distances r'. This is the same method previously described by Kars and Wallinga [25], and it is used in all the FSF developed in this paper.

Equation (21) can be interpreted as the sum of several saturating exponential functions of the form $A\left(1-\exp\left(-\lambda t\right)\right)$. Each of these exponentials has a different amplitude $A\left(r'\right)=g(r')\dot{D}/\left[D_0 s_{eff}\left(r'\right)+\dot{D}\right]$, and different decay constants $\lambda(r')=\dot{D}/D_0+s_{eff}\left(r'\right)$.

Typical values of the parameters used in the simulations by Li and Li [23] are $\rho'=2\times10^{-6}$, $s=3\times10^{15}$ s^{-1}, $\dot{D}=3$ Gy ka^{-1}, and $D_0=538$ Gy.

The simplified minimal code in Listing 2 simulates this irradiation process by using the function *irradfortimeT()*, which evaluates the distribution of nearest neighbor distances at the end of the irradiation process. The overall structure of the code in Listing 2 is kept identical to the structure of Listing 1, so that the users can readily follow and modify the

code for their purposes. Lines 2-6 define the parameters ρ', D_0, $\dot{D}$, r' and s. Lines 7 and 8 evaluate the three different irradiation times in seconds, and line 9 is the unfaded nearest neighbor distribution from Eq.(5).

Lines 11-13 are similar to the corresponding lines in Listing 1. These lines define again the matrix ***distribs*** which contains four columns corresponding to the four geological times, and ***matplot()*** is used plot the distributions at the end of the irradiation times.

The results of the code are shown in Fig.6, and they are identical to Fig.5a in the paper by Li and Li [23]. As the irradiation time increases, Fig.6 shows that the asymmetric distribution of distances r' approaches the distribution for a field saturated sample ($\times$ symbols). The symmetric curve indicates the initial distribution of distances for the unfaded sample (o symbols) at time $t = 0$.

```
1  source("Functions_FSFpaper.R")                    # Load the FSF R-codes
2  rho <- 2e-6                                       # dimensionless acceptor density
3  D0 <- 538                                         # D0 in Gy
4  Ddot <- 3                                         # low natural dose rate in Gy/ka
5  rprimes <- seq(0.01, 2.2,.01)                     # r'=0-2.2, step .01
6  s <- 2e+15                                        # frequency factors in s^-1
7  yr <- 3.15576e+7                                  # set year in seconds
8  irrTimes <- c(6.67e4, 1.67e5, 1e6) * yr           # irradiation times
9  unfaded <- 3 * rprimes ^ 2 * exp(-rprimes ^ 3)    # unfaded sample
10
11 distribs <- irradfortimeT(irrTimes, rprimes, rho, s, Ddot, D0)
12 matplot(rprimes, distribs)
13 lines(rprimes, unfaded)
14
15 plot(irrTimes / yr, colSums(distribs) * 0.1)
```

LISTING 2

R code demonstrating the function ***irradfortimeT()*** to simulate the distribution of distances in the IGST model in Fig.2b.

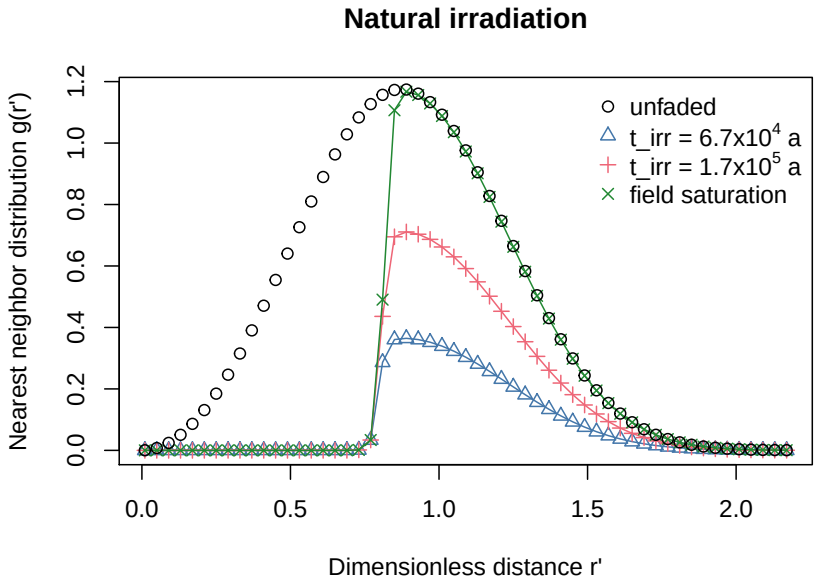

Figure 5: Simulation of irradiation process in nature, using the FSF *irradfortimeT()*. As the irradiation time increases, the asymmetric distribution of distances r' approaches the field saturation distribution ($\times$ symbols). The symmetric curve indicates the initial distribution of distances, for the unfaded sample (o symbols). For additional examples of this type of simulation, see the papers by Li and Li [23], and Kars and Wallinga [25].

Figures 6 and 7 shows the result of simulating the irradiation process and the measurements of the dose response curves in nature and in the laboratory, respectively. By using the extra line 15 in Listing 2, we obtain the dose response plot shown in Fig.6.

In the simulations of Fig.7, the laboratory irradiations are of course carried out with a much higher dose rate of 0.1 Gy s^{-1}, and for much shorter irradiation times $t_{irr} = 1 - 10^6$ s. As the irradiation time increases in both Figs.6 and 7, both the asymmetric distribution of distances r' and the trap filling ratio $n(t)/N$ approach the saturation distribution for a field saturated sample.

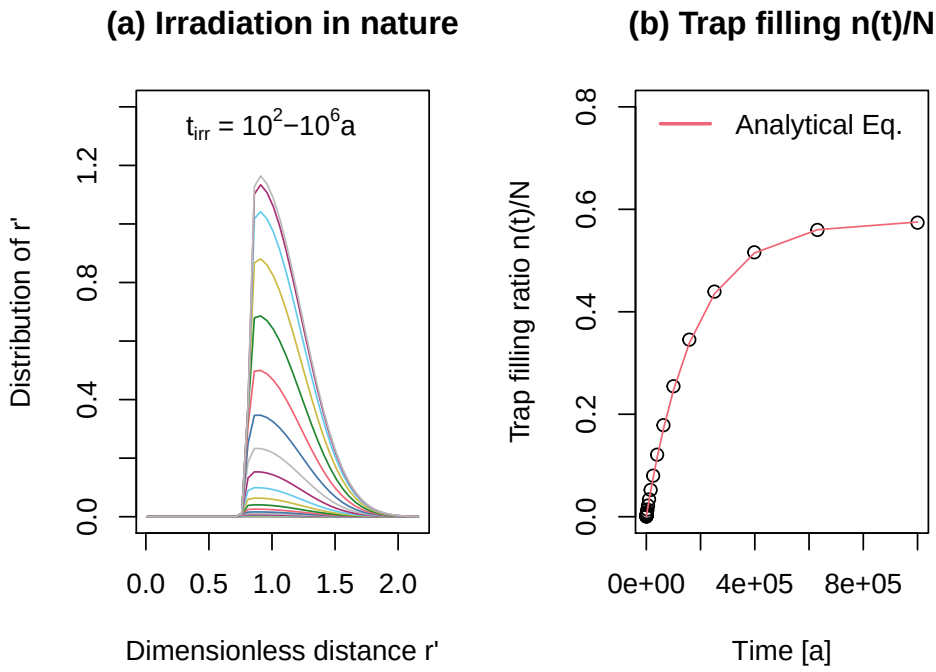

Figure 6: Simulation of irradiation process in nature with a low dose rate of 3 Gy ka^{-1}, using the FSF *irradfortimeT()*. (a) As the irradiation time increases, the asymmetric distribution of distances r' approaches the field saturation distribution. (b) The corresponding dose response curve. For additional examples of dose response curves based on this model, see Li and Li [23], and Kars and Wallinga [25].

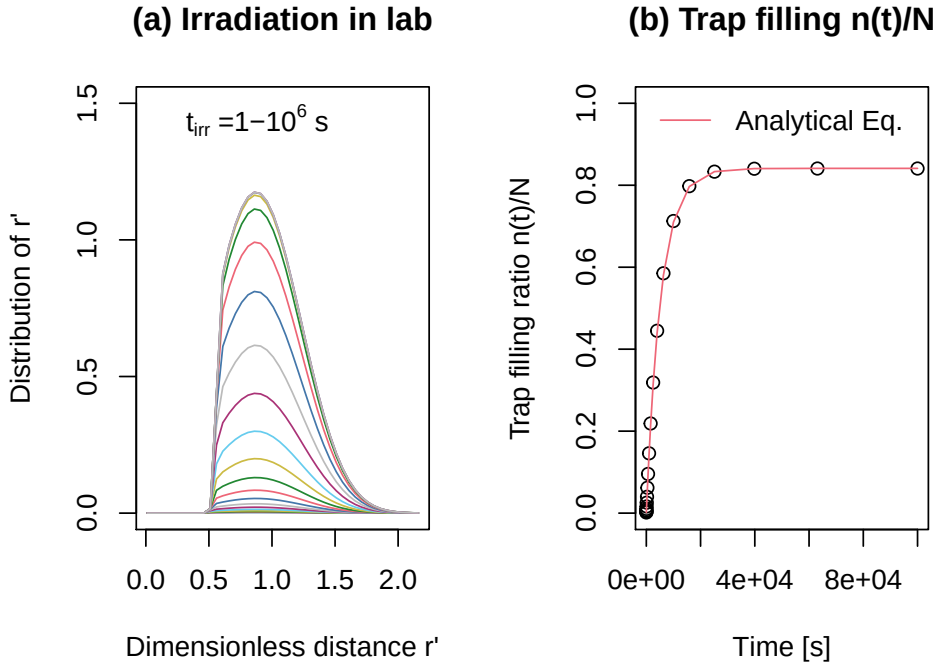

Figure 7: Simulation of irradiation process in the *laboratory*, using the FSF *irradfortimeT()*. The dose rate is 0.1 Gy s^{-1} and the irradiation times $t_{irr} = 1 - 10^6$ s. As the irradiation time increases, both the asymmetric distribution of distances r' in (a), and the trap filling ratio $n(t)/N$ in (b) approach saturation.

We can compare the results in Figs.6 and 7, with the analytical equation developed by Pagonis and Kitis [34]. These authors showed that the integral equations for the dose response curves in the model of Li and Li [23] can be replaced with the following approximate analytical equation:

$$L_{\text{FADED}}(D) = N\left(1 - \exp\left[-D/D_0\right]\right) \exp\left[-\rho' \ln\left(\frac{D_0 s}{\dot{D}}\right)^3\right] \tag{22}$$

where the saturating exponential term $N\left(1 - \exp\left[-D/D_0\right]\right)$ represents the luminescence signal that would have been obtained in the absence of any fading.

A plot of this equation is shown by the solid lines in Figs.6 and 7, showing excellent agreement between the analytical equation (22) and the R functions developed in this paper.

7. Quantum tunneling from the excited state of the electron trap

The previous two sections discussed the simple GST and IGST models, which are based on quantum tunneling taking place from the ground state of the trapped electron. In this section we discuss a different type of model, which is based on tunneling occurring from the excited state of the trap, shown in Fig.2c.

Experimental work on feldspars has shown the existence of two different ranges of values of the dimensionless acceptor density ρ', which characterizes feldspars. One observes either a low value of the density $\rho' \sim 10^{-6}$, which explains anomalous fading phenomena (see for example Li and Li [23]), or a much higher value of $\rho' \sim 10^{-3}$ which is associated with excited state tunneling phenomena. For example, Pagonis et al. [35] carried out a detailed experimental study of the CW-IRSL signals in 23 feldspar samples, and found that these signals are described by a narrow range of the dimensionless acceptor density $\rho' = 0.002 - 0.01$. Further extensive experimental work on a suite of 10 feldspars has been carried out by Sfampa et al. [36, 37], Kitis et al. [38] and Sahiner et al. [39] who found similar ranges of values for the parameter ρ' from the analysis of TL and CW-IRSL signals.

Pagonis et al. [40] discussed the physical basis of these two ranges of values of the dimensionless density ρ'. Low values of $\rho' = 10^{-6}$ are most likely due to a small value of the tunneling constants $a = 0.2$ nm in Eq.(1). Similarly, high values of $\rho' = 10^{-3}$ may be due to much larger tunneling constants a in Eq.(1), of the order of $a = 2$ nm. For a discussion of the crystal structure and of the extent of the corresponding wavefunctions in feldspars, the reader is referred to two papers by Poolton ([41, 20]).

Jain et al. ([13],[42]) developed mathematically the EST model in Fig.2c. Pagonis et al. [33] discussed quantum tunneling in this model, and noted that the rate of loss of trapped

charge is given by:

$$\frac{\partial n\left(r',t\right)}{\partial t}=-n\left(r',t\right)\frac{A\left(t\right)s_{tun}}{B}\exp\left[-\left(\rho'\right)^{-1/3}r'\right] \tag{23}$$

where $A(t)$ (s^{-1}) is the rate of optical or thermal excitation from the ground state to the excited state of the trapped electron, B (s^{-1}) is the rate of retrapping from the excited to the ground state, and s_{tun} (s^{-1}) represents the tunneling frequency from the excited state into the recombination center. As in the other models of this paper, $n(r',t)$ is the concentration of trapped electrons at time t and at a distance r', and ρ' is the constant dimensionless density of acceptors in the material.

Equation (23) is a first order differential equation for a fixed distance r', and its solution is:

$$n\left(r',t\right)=Ng\left(r'\right)\exp\left\{-\frac{s_{tun}}{B}\exp\left[-\left(\rho'\right)^{-1/3}r'\right]\int_{0}^{t}A\left(t\right)dt\right\} \tag{24}$$

The excitation rate $A(t)$ is different for various types of experiments (TL, CW-IRSL, isothermal TL, etc.), and is discussed in the next two sections.

The total concentration of trapped electrons at time t is found by integrating over all distances r':

$$n(t)=\int_{0}^{\infty}n\left(r',t\right)dr'=\int_{0}^{\infty}Ng\left(r'\right)\exp\left\{-\frac{s_{tun}}{B}\exp\left[-\left(\rho'\right)^{-1/3}r'\right]\int_{0}^{t}A\left(t\right)dt\right\}dr' \tag{25}$$

In these types of experiments, the time-dependent luminescence intensity $I(t)$ is evaluated numerically by integrating the rate of change of the concentration over all possible values of the variable r':

$$I\left(t\right)=-\int_{0}^{\infty}\frac{\partial n\left(r',t\right)}{\partial t}dr' \tag{26}$$

Once $n(r',t)$ is evaluated using the above Eq.(24), we can evaluate $I(t)$ by combining Eqs.(23) and (26):

$$I\left(t\right)=\int_{0}^{\infty}n\left(r',t\right)\frac{A\left(t\right)s_{tun}}{B}\exp\left[-\left(\rho'\right)^{-1/3}r'\right]dr' \tag{27}$$

In all these different types of experiments, the FSF replace the numerical integrations with appropriate sums.

8. Simulation of CW-IRSL curves of unfaded samples

In a CW-IRSL experiment, the rate of excitation is given by $A_{CW} = \sigma I$, where σ (cm^2) represents the optical cross section for the process, and I ($\mathrm{cm}^{-2}\mathrm{s}^{-1}$) is the intensity of the excitation IR source. For these types of experiment, Eq.(24) becomes:

$$n_{CW}\left(r',t\right) = N\, g\left(r'\right) \exp\left\{-\frac{s_{tun}\sigma I}{B} \exp\left[-\left(\rho'\right)^{-1/3} r'\right] t\right\} \tag{28}$$

$$n_{CW}\left(r',t\right) = 3N\ \left(r'\right)^2 \exp\left[-\left(r'\right)^3\right] \exp\left\{-A_{eff}(r')\, t\right\} \tag{29}$$

where we defined an effective infrared excitation rate $A_{eff}(r')$ (s^{-1}) for the CW-IRSL process, given by:

$$A_{eff}(r') = \frac{s_{tun}\sigma I}{B} \exp\left[-\left(\rho'\right)^{-1/3} r'\right] \tag{30}$$

In the R codes we will replace the combination of frequency factors σI, s_{tun}, B with a frequency $s = s_{tun}\sigma I/B$. This does not affect the simulations, since these three factors appear as the combination $s_{tun}\sigma I/B$ in the model, and not separately. In this case, s represents an effective total frequency factor of the CW-IRSL process in this model.

The total concentration of trapped electrons at time t is found by integrating over all distances r':

$$n(t) = \int_0^\infty n\left(r',t\right) dr' = \int_0^\infty N g\left(r'\right) \exp\left\{-A_{eff}(r')\, t\right\} dr' \tag{31}$$

This equation can again be regarded as the sum of many exponentials for different r' values, with amplitudes $3\left(r'\right)^2 \exp\left[-\left(r'\right)^3\right]$, and decay constants $A_{eff}(r')$. One can then evaluate $n(t)$ during the CW-IRSL experiment by adding the exponentials in this form:

$$n(t) = N \sum_{r'=0}^{r'=2.2} 3\left(r'\right)^2 \exp\left[-\left(r'\right)^3\right] \exp\left[-A_{\mathrm{eff}}\left(r'\right) t\right] \Delta r' \tag{32}$$

```
1  source("Functions_FSFpaper.R")                    # Load the FSF R-code
2  ## define parameters
3  rho <- .013                                       # dimensionless acceptor density
4  dr <- .05                                         # step in dimensionless distance r
5  rprimes <- seq(0, 2.2, dr)                        # r'=0-2.2 in steps of dr
6  A <- 3                                            # A=stun*sigma*I/B
7  timesCW <- seq(1, 100)                            # IR excitation times
8
9  ## calculate
10 distr <- 3 * rprimes ^ 2 * exp(-rprimes ^ 3)      # unfaded distribution
11 afterIRSL_distr <- CWfortimeT(max(timesCW), rho, rprimes, A)
12 IRsignal <- stimIRSL(timesCW, rho, rprimes, A, distr) # CW-IRSL signal
13 CWcurves <- t(CWsignal(timesCW, rho, rprimes, A, distr))
14
15 ## plotting
16 par(mfrow = c(1, 3))
17 plot(rprimes, distr)                              # plot unfaded distribution
18 lines(rprimes, afterIRSL_distr)                   # distribution after IR
19 matplot(timesCW, CWcurves)                       # plot many CW curves
20 plot(timesCW, IRsignal)
```

LISTING 3

Example of using three FSF *CWfortimeT()*, *stimIRSL()* and *CWsignal()* to evaluate the distributions $n(r', t)$ and the CW-IRSL signal from freshly irradiated samples, within the EST model in Fig.2c.

Listing 3 shows an example of using the three R functions *CWfortimeT()*, *stimIRSL()* and *CWsignal()*, to simulate a CW-IRSL experiment. An example of running the code is shown in Fig.8. The structure of the overall R code in Listing 3 is very similar to the structure in Listings 1 and 2, for purposes of clarity.

Lines 3-6 of the code in Listing 3 set the values of the input parameters, and line 7 contains the parameter *timesCW* for the time period of the CW-IRSL simulation (1-100 s). Line 10 defines the unfaded distribution of distances, and Line 11 calls the function *CWfortimeT()*, which evaluates the new distribution of charges $n(r', t)$ at the end of the CW-IRSL experiment. Lines 12-13 calls the function *stimIRSL()* and *CWsignal()* to evaluate the CW-IRSL intensity. The signal is stored in the parameter *CWcurves* representing the partial CW-IRSL curves shown in Fig.8b.

Line 18 plots the *new* distribution of charges $n(r', t)$ at the end of the CW-IRSL exper-

iment. Line 19 uses *matplot()* to plot all the individual exponential decay curves corresponding to different values of r', and finally Line 20 plots the sum of the curves.

The solid line in Fig.8(c) is the approximate analytical KP-CW equation developed by Kitis and Pagonis [43]; this equation is discussed further in section 12.

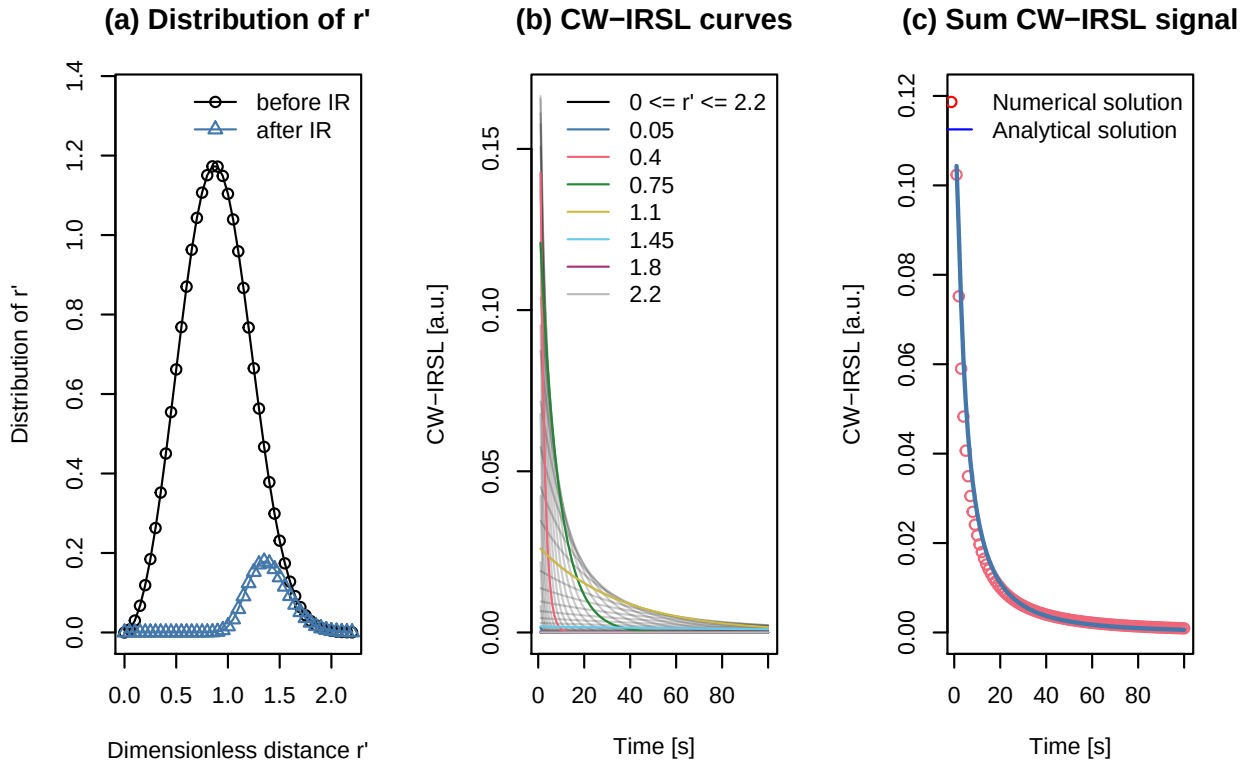

Figure 8: Simulation of CW-IRSL experiment for freshly irradiated samples, using the three FSF *CWfortimeT()*, *stimIRSL()* and *CWsignal()*. (a) The distributions of distances at the beginning and at the end of the CW-IRSL experiment ; (b) The CW-IRSL curves evaluated for each distance r'; (c) The sum of the curves shown in (b) yields the total CW-IRSL signal. The solid line in (c) is the analytical KP-CW equation developed by Kitis and Pagonis [43]. The parameters in the model are typical for feldspars, A =3.0 s^{-1}, ρ'=0.013.

9. Simulation of TL glow curves in freshly irradiated samples

In a TL experiment, the rate of excitation is given by $A_{TL}(t) = s_{th} \exp[-E/(k_B T)]$, where s_{th} (s^{-1}) and E (eV) are the thermal frequency factor and the activation energy of the trap respectively, and T (K) is the temperature of the sample. For a TL experiment, Eq.(24) becomes:

$$n_{TL}(r', t) = N\, g(r') \exp\left\{ -\frac{s_{tun} s_{th}}{B} \exp\left[-(\rho')^{-1/3} r' \right] \int_0^t \exp[-E/(k_B T)]\, dt \right\} \qquad (33)$$

$$n_{TL}\left(r',t\right)=N\,g\left(r'\right)\exp\left\{-s_{\text{eff}}\left(r'\right)\int_{0}^{t}\exp\left[-E/(k_{B}T)\right]dt\right\} \tag{34}$$

where we defined an effective frequency factor $s_{\text{eff}}\left(r'\right)$ (s^{-1}) for the TL process, given by:

$$s_{\text{eff}}\left(r'\right)=\frac{s_{tun}s_{th}}{B}\exp\left[-\left(\rho'\right)^{-1/3}r'\right] \tag{35}$$

Pagonis et al. [33] noted that the TL signal from feldspars can be calculated as the sum of several partial TL glow curves, with each of these partial TL glow curves corresponding to a different distance r'. Just as in the case of the CW-IRSL curves described in the previous section, the amplitude of these TL glow curves is proportional to the nearest neighbor distribution $3\left(r'\right)^{2}\exp\left[-\left(r'\right)^{3}\right]$, and the respective effective frequency constants $s_{eff}\left(r'\right)$ are given by Eq.(35).

Just as in the previous section, we will replace the combination of frequency factors s_{th},s_{tun},B in the R code with a frequency $s=s_{th}s_{tun}/B$. This will not affect the simulations, since these three frequencies appear as the combination $s_{th}s_{tun}/B$ in the model; in this case, the parameter s is a total effective frequency factor, representative of the TL process in this model.

In the code which follows, we simulate the process by using again a summation over the different r' values, instead of a formal integration. By contrast to the CW-IRSL code in the previous section, instead of adding many exponentials, we are now adding many first order TL peaks. For an implementation of this method using a Monte Carlo method, see Figure 7 in Pagonis et al. [33]. In the R code, the first order glow peaks will be added, thus:

$$I(t)=N\sum_{r'=0}^{r'=2.2}3\left(r'\right)^{2}\exp\left[\left(r'\right)^{3}\right]s_{eff}\left(r'\right)e^{-E/k_{B}T}\exp\left[-s_{eff}\left(r'\right)\int_{0}^{t}e^{-E/k_{B}T}dt'\right] \tag{36}$$

The integral appearing in this equation will be approximated using the following well-known expression for the exponential integral when using a linear heating rate β (see for example the book by Chen and Pagonis [1]):

$$\int_{0}^{t}e^{-E/kT}dt'=\frac{k_{B}T^{2}}{E}\left[\exp\left(-\frac{E}{k_{B}T}\right)\left(1-\frac{2k_{B}T}{E}\right)\right] \tag{37}$$

Listing 4 shows an example of using the R function `stimTL()` to simulate a TL experiment. An example of running the code is shown in Fig.9. The structure of the overall R

code in Listing 4 is again kept similar to the structure in Listings 1-3, for clarity. The model parameters in these simulations are $\rho' = 0.013$, $E = 1.45$eV, $s = 3.5 \times 10^{12}$ s^{-1}.

Figure 9 shows a simulation of heating a sample up to 400°C, just below the high temperature end of the TL glow curve. Fig.9a shows the distributions of distances r' before and after heating the sample. The circles indicate the initial unfaded distribution before the heating, and the triangles indicate the corresponding distribution after heating to 400°C. As may be expected, after heating to 400°C, only a few distant electrons remain trapped in the sample, corresponding to large values of $r' > 1.3$.

Fig.9b shows the partial TL glow curves, which are summed to produce the very broad glow curve in Fig.9c.

```
source("Functions_FSFpaper.R")                    # Load the FSF R-code
## set parameters
dr <- .1                                          # step in dimensionless dist. r
rprimes <- seq(0.01, 2.2, dr)                     # r'=0-2.2, steps of dr
rho <- .013                                       # dimensionless acceptor density
s <- 3.5e+12                                      # frequency factors in s^-1
E <- 1.45                                         # energy in eV
seff <- s * exp(-rprimes * (rho ^ (-1 / 3.0)))    # effective s
beta <- 1                                         # heating rate (K s^-1)
temp <- 1:400                                     # temperatures for TL

## calculate TL signal and plot
TL <- stimTL(temp, E, s, rho, rprimes)
plot(temp, TL)
```

LISTING 4

Example of using the FSF *stimTL()* to evaluate the distributions $n(r', t)$ and the TL signal from freshly irradiated samples, within the EST model in Fig.2c.

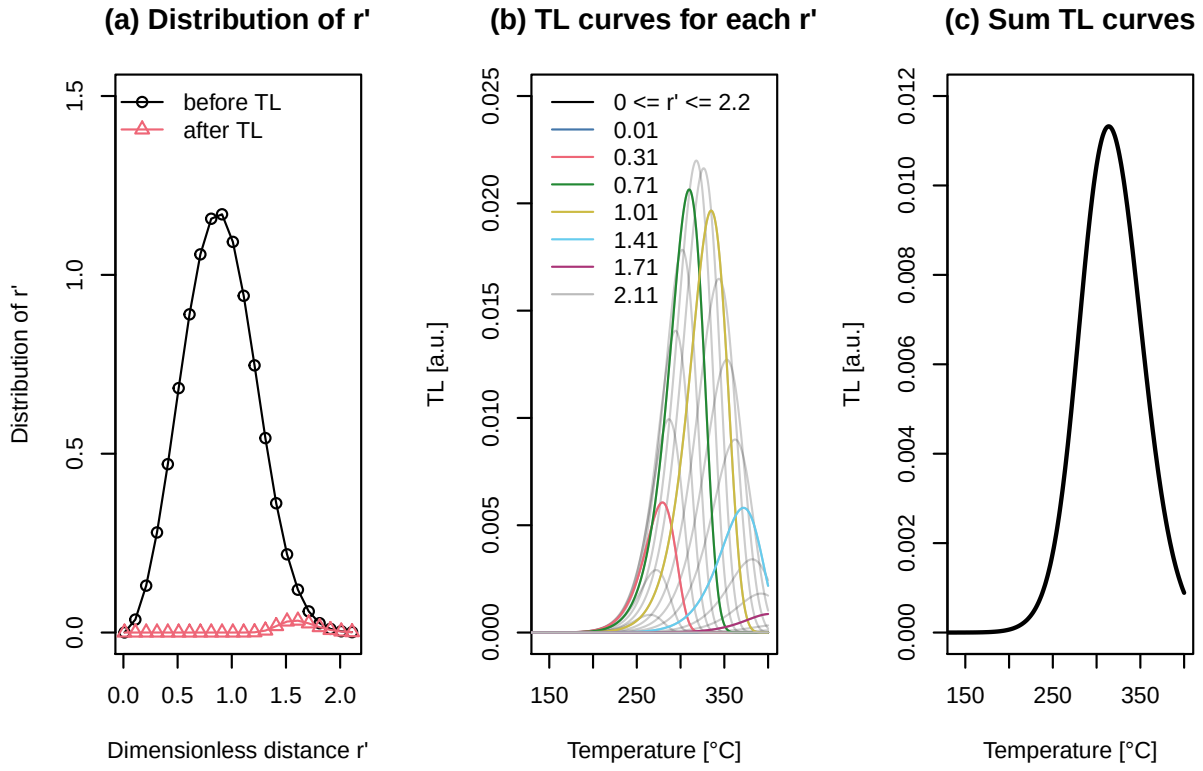

Figure 9: Simulation of TL glow curve for freshly irradiated samples using the FSF *stimTL()*. The sample is heated up to 400°C, just below the high temperature end of the TL glow curve. (a) The distributions of distances r' before and after the heating the sample are shown as circles and triangles, respectively; (b) The partial first order TL glow curves; (c) The sum of the glow curves from (b). The model parameters are $\rho' = 0.013$, $E = 1.45$eV, $s = 3.5 \times 10^{12}$ s^{-1}.

10. TL signals from thermally and optically treated samples

Luminescence dosimetry laboratories often use complex experimental protocols, consisting of combinations of irradiations, and/or thermal and optical treatments of the samples. Such complex sequences of events can be simulated by following the development of the distribution of nearest neighbor distances in successive stages of the experiment.

For example, Polymeris et al. [7] followed the development of these distributions in successive stages of the experiment, and described quantitatively the changes taking place in the experimental TL glow curves for four types of preheated feldspar samples; an orthoclase, a sanidine and two microclines. Both the preheat temperature and the duration of the preheat were varied in the experiments, before measurement of the remnant TL glow curve. In a more recent study, Pagonis et al. [8] presented a comprehensive analysis of TL signals in MgB_4O_7:Dy,Na dosimeters, based on the TA-EST model shown in Fig.2c. Their simulations

provided a quantitative description of the TL signals in this material, following a wide variety of thermal treatments.

The FSF in this paper can describe such complex sequences of irradiation, thermal and optical excitation, with an example shown in the curves 1-4 of Fig.10. These curves correspond to the following experimental situations, respectively:

1. TL for freshly irradiated sample (unfaded distribution of distances r').
2. Sample freshly irradiated, then heated to a preheat temperature $Tph = 320$°C, then TL measurement. This example uses the two FSF ***heatTo()*** and ***stimTL()***.
3. Sample freshly irradiated, then preheated for time $tph = 30$ s at a preheat temperature $Tph = 320$°C, then TL measurement. This example uses the three FSF ***heatTo()***, ***heatAt()*** and ***stimTL()***.
4. Sample freshly irradiated, then CW-IRSL excitation for 50 s, then TL measurement. This example uses sequentially the two FSF ***CWfortimeT()*** and ***stimTL()***.

Fig.10a shows the distributions of nearest neighbor distances before measurement of the TL glow curve in these 4 examples, while Fig.10b shows the corresponding TL glow curves for each simulation. The parameters in these models are typical for feldspars.

Listing 5 shows the code used to produce curve 2 in Fig.10.

```
source("Functions_FSFpaper.R")                    # Load the FSF R-code
## set parameters
rho <- .013              # dimensionless acceptor density
s <- 3.5e12              # frequency factors in s^-1
E <- 1.45                # energy in eV
Tph <- 320               # preheat Temperature (deg C)
temps <- 1:400           # TL temperature
rprimes <- seq(0.01, 2.2, 0.05) # values of r'=0-2.2 in steps of dr
beta <- 1

## simulation and plotting
distr <- heatTo(Tph, E, s, beta, rho, rprimes)     # heat to 320 deg C
TL <- stimTL(temps, E, s, rho, rprimes, distr = distr)
plot(temps, TL)
```

LISTING 5

Example of using the FSF to simulate heating a freshly irradiated sample up to a preheat temperature T_{PH}, then measure TL, within the EST model in Fig.2c.

Fig.10 shows a general property of the TL glow curves in pretreated feldspar samples; the relative shape and location of the TL glow curves along the temperature axis reflects the underlying similar behavior of the distributions of distances r'. However, note that the horizontal axis in Fig.10a (distance r'), is physically very different from the x-axis in Fig.10b (sample temperature). This similarity in the shapes of the TL glow curves and the distribution of distances r' is discussed in detail in Pagonis and Brown [44].

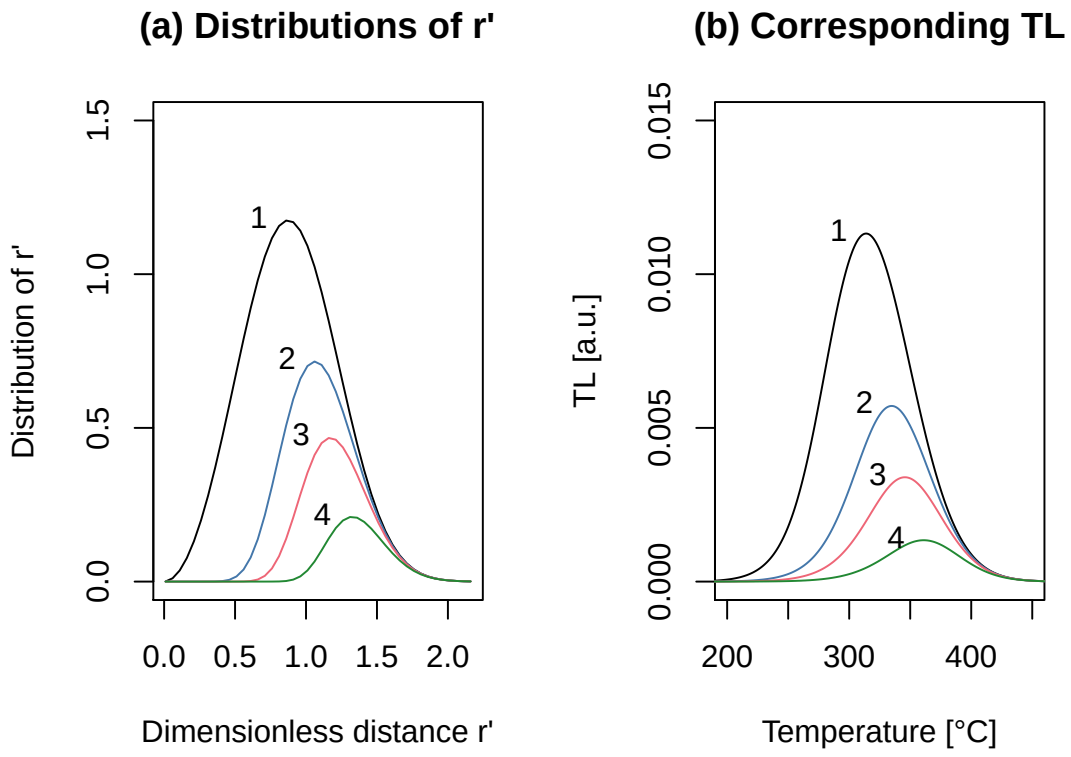

Figure 10: Several examples of the simulation functions for thermally and optically treated samples, using the FSF . The parameters in the model are typical for feldspars. (1) TL for unfaded sample; (2) Heat to temperature T_{PH}=320°C, then measure TL; (3) Heat for 30 s at T_{PH}=320°C, then measure TL; (4) CW-IRSL excitation for 50 s, then measure TL.

11. The low temperature thermochronometry model by Brown et al.

Brown et al.[9] investigated the simultaneous effects of irradiation and quantum tunneling on the TL glow curves in materials within a random distribution of defects. These authors extended the original model by Jain et al. [42, 13] and Li and Li [23], to include all three processes: irradiation, quantum tunneling and thermally assisted processes. This FOK model was developed for low temperature thermochronometry, however it is completely general and can be used for any thermally active dosimetric trap. The model is based on the following

differential equation:

$$\frac{\partial n\left(r',t\right)}{\partial t}=\frac{\dot{D}}{D_0}\left[N\left(r'\right)-n\left(r',t\right)\right]-n\left(r',t\right)\exp\left(-\frac{E}{k_BT}\right)\frac{P\left(r'\right)s}{P\left(r'\right)+s} \tag{38}$$

where $P(r')$ is the rate of excited state tunneling given by:

$$P(r')=P_0\exp\left[-\left(\rho'\right)^{-1/3}r'\right] \tag{39}$$

The parameters in this model are the tunneling frequency P_0 (s^{-1}), T represents the temperature of the sample, k_B is the Boltzmann constant, s (s^{-1}) is the trap frequency factor and E (eV) is the thermal activation energy of the trap from the ground state to a higher energy unspecified state. In order to simplify the notation, we can now define an effective tunneling probability $P_{eff}\left(r'\right)$ which depends also on the sample temperature T:

$$P_{eff}\left(r'\right)=\frac{P\left(r'\right)s}{P\left(r'\right)+s}\exp\left[-E/\left(k_BT\right)\right] \tag{40}$$

The solution of the first order differential Eq.(38) for a constant r' is the following simple saturating exponential function:

$$n\left(r',t\right)=\frac{\dot{D}\,N\,g\left(r'\right)}{D_0\,P_{eff}\left(r'\right)+\dot{D}}\left[1-\exp\left\{-\frac{\dot{D}}{D_0}+P_{eff}\left(r'\right)\,t\right\}\right] \tag{41}$$

This is the *new* partial analytical solution for the TA-EST model by Brown et al. [9]. It is mathematically similar to the analytical solutions Eq.(10), (18) and (24) for the GST, IGST and EST model, respectively. By using this analytical expression, it is possible to replace the double numerical integration shown in Eq.(7) with a summation over the finite range of the distance parameter r'.

As a first example, we simulate in Fig.11 the dose response during natural irradiation. We simulate multiple irradiations in nature, by using the function *irradandThermalfortimeT()*, to describe the trap filling process for various irradiation times t_{irr}, and for a fixed steady state temperature $T_{IRR}=-4$°C. The result is shown in Fig.11. As the irradiation time increases, the distribution of trapped electrons $n\left(r',t\right)$ at the end of the irradiation shifts toward higher distances and increases overall, eventually reaching the distribution of the field saturated sample.

It must be noted that Brown et al. [9] used a value of $\rho'=0.00132$, which is three orders of magnitude larger than the ground state tunneling value of $\rho'=10^{-6}$. It is also noted that this model contains two frequency factors s and P_0, while the excited state Eq.(35)

introduced previously in this paper contains a single effective frequency factor $s_{eff}(r')$. The input parameters in this TA-EST model are ρ', P_0, E , s , D_0, $\dot{D}$, T_{irr} and t_{irr}.

From a physical point of view, it is very interesting to compare the shape of the distributions in Fig.11 with those from Fig.6, which were obtained using a much lower value of the acceptor density parameter $\rho' = 10^{-6}$ and for a thermally stable trap. In Fig.11 the critical radius r'_c is not as pronounced and well defined as in Fig.6.

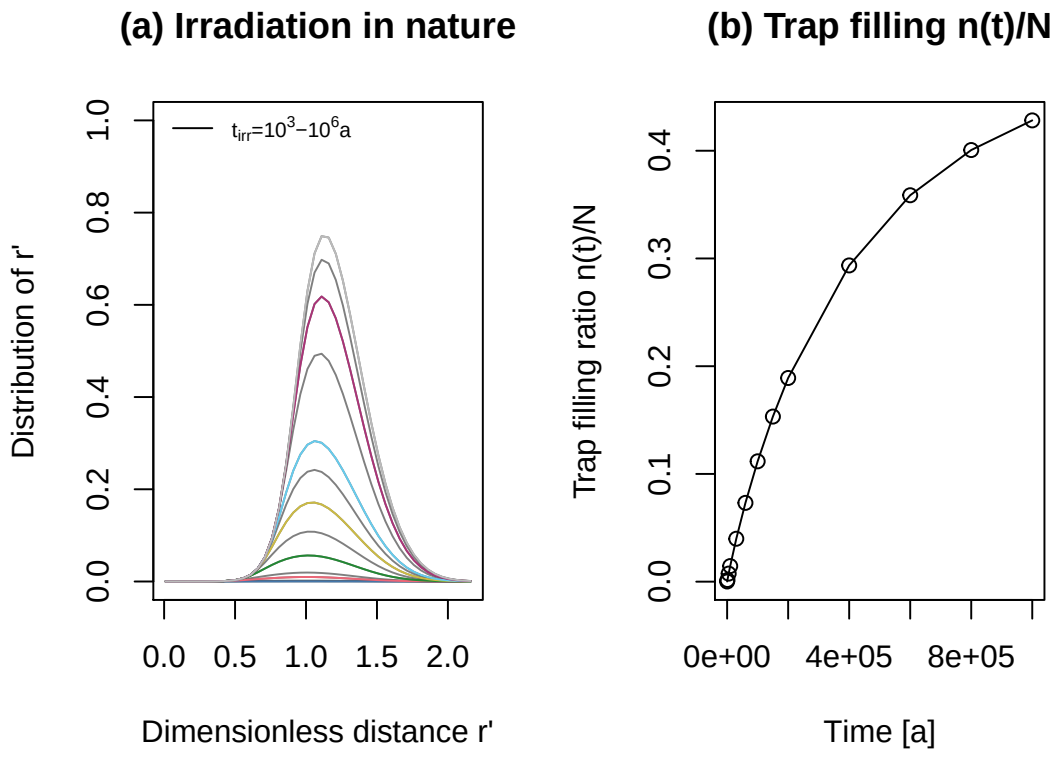

Figure 11: Simulation of irradiations in nature using the FSF *irradandThermalfortimeT()* in the TA-EST model, for a fixed steady state temperature of -4°C. (a) The distributions of the distance parameter r' at various irradiation times. Compare the shape of these distributions with Fig.6. (b) The corresponding dose response shown as the trap filling ratio $n(t)/N$. For further examples of this type of simulation, the reader is referred to Brown et al. [9].

We next simulate multiple irradiations in nature, with variable steady state temperatures $T_{irr} = -4, 0, 4, 8^\circ$ C, and for a fixed irradiation time $t_{irr} = 10^3$ a, with the result shown in Fig.12. As the steady state temperature increases, the distribution of trapped electrons $n\,(r', t)$ at the end of the irradiation shifts toward higher distances and decreases overall. This is because more thermally assisted tunneling takes place at elevated steady-state temperatures; the closest neighbors recombine first in time, and the overall distribution shifts to higher values of r'.

Similar results for the effect of steady state temperature on the TL glow curve were obtained in the extensive experimental and modeling work by Brown et al. ([45, 9]),

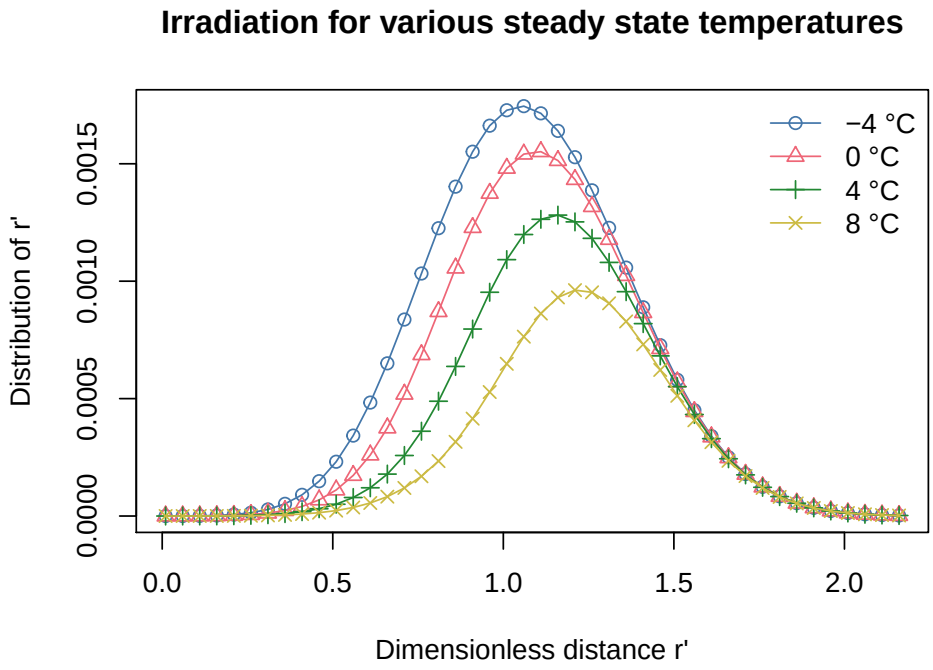

Figure 12: Multiple irradiations in nature using the FSF *irradatsometemp()* in the TA-EST model, for variable burial temperatures T_{irr}= -4, 0, 4, 8 °C and for a fixed irradiation time $t_{irr} = 10^3$ a. For further examples, see Brown et al. [9].

12. The Kitis-Pagonis analytical solution of the EST model

From a practical point of view, researchers are interested in how to extract the parameters in the model from the experimental data. For example, how does one extract the values of the dimensionless acceptor density ρ' from the experimental CW-IRSL and TL curves in feldspars? Establishing reliable values for these parameters is an important part for both modeling and for further experimental studies of these materials.

In this section, we present two least squares fitting R codes, which can be used to fit experimental CW-IRSL and TL data for freshly irradiated feldspar samples. To the best of our knowledge, these are the first published computer scripts for the analysis of CW-IRSL and TL signals in feldspars.

Kitis and Pagonis [43] derived an analytical equation for the model by Jain et al. [13], by considering quasi-equilibrium conditions (QE). These authors obtained the following analyt-

ical solutions for the concentration of electrons $n(t)$ during a CW-IRSL or TL experiment:

$$n(t) = n_0 \exp\left(-\rho' \ln\left[1 + z \int_0^t p(t)\, dt\right)\right]^3\right)$$

where $p(t)$ (s^{-1}) is the appropriate excitation rate for each thermal/optical stimulation experiment. The corresponding luminescence intensity $I(t)$ is found from the derivative $-dn/dt$:

$$I(t) = 3\, n_0\, \rho'\, z\, p(t)\, F(t)^2\, e^{-F(t)}\, e^{-\rho'(F(t))^3} \tag{42}$$

$$F(t) = \ln\left(1 + z \int_0^t p(t)\, dt\right) \tag{43}$$

For practical work of fitting experimental CW-IRSL data, we use these equations in the following form, which in this paper will be referred to as the *Kitis-Pagonis CW-equation (KP-CW):*

$$I_{\text{CW-IRSL}}(t) = \frac{I_0\, F(t)^2\, e^{-\rho'(F(t))^3}}{1 + zA\, t} + bgd \tag{44}$$

$$F_{\text{CW-IRSL}}(t) = \ln\left(1 + zA\, t\right) \tag{45}$$

where z =1.8 and the fitting parameters are A, I_0, ρ' and a constant background bgd. Several experimental studies have found that typical values of the infrared stimulation rate A are 1-10 s^{-1}, and that for CW-IRSL and TL signals in feldspars the typical values of the dimensionless density $\rho' = 0.003 - 0.02$ (see for example the previously mentioned comprehensive studies by Pagonis et al. [35], Sfampa et al. [36, 37], Kitis et al. [38] and Sahiner et al. [39]).

The best fitting parameters obtained from the least squares fitting for the data in Fig.13 are I_{max} =2.72×10^4 cts s^{-1}, A =7.07 s^{-1}, ρ'=0.0073 and the background bgd =47.05 cts s^{-1}.

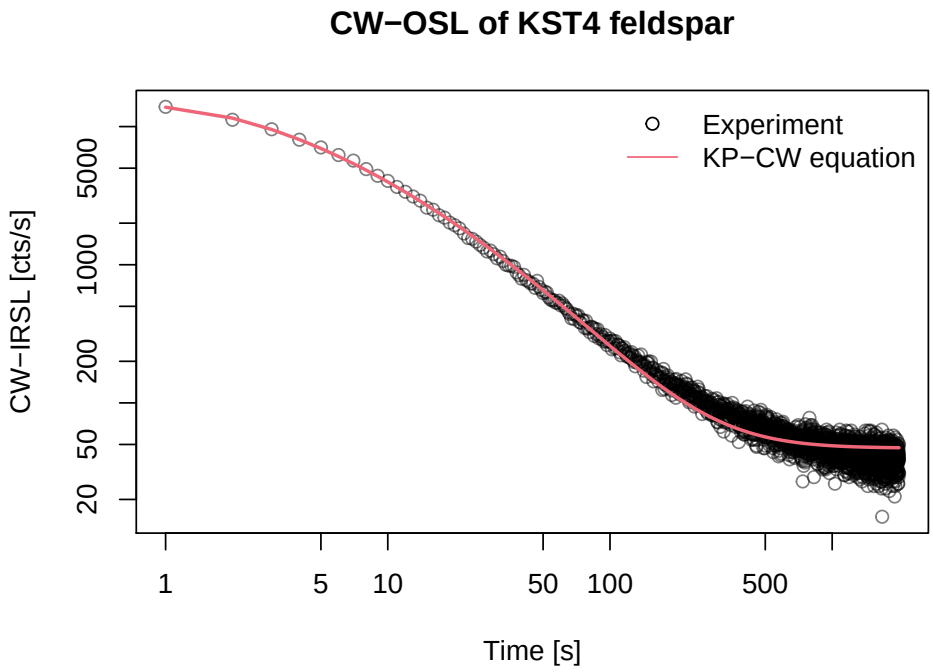

Figure 13: Experimental CW-IRSL glow curves from freshly irradiated KST4 feldspar sample, fitted using the Kitis-Pagonis analytical Eq.(44). For more details, see Pagonis et al. [33].

For freshly irradiated samples, the TL signals are analyzed using the following *KP-TL* equation for the intensity of a TL signal (see equations (29) and (30) in Kitis and Pagonis [43]):

$$I_{\mathrm{TL}}(t) = \frac{I_0\, F(t)^2\, e^{-\rho'(F(t))^3}\, (E^2 - 6k_B^2T^2)}{Ek_BsT^2z - 2k_B^2sT^3z + \exp\left(E/k_BT\right) E\beta} + bgd \tag{46}$$

$$F_{\mathrm{TL}}(t) = \ln\left(1 + \frac{z\, s\, k_BT^2}{\beta E}\, e^{-\frac{E}{k_BT}} \left(1 - \frac{2k_BT}{E}\right)\right) \tag{47}$$

and the fitting parameters are I_0, E, s, I_0, ρ', bgd. Here β is the constant heating rate. Even though these equations look rather complex, they are easy to code.

In order to constrain the code using experimental data, we use the known value of E =1.45 eV, obtained from separate initial rise and $T_{\mathrm{max}} - T_{\mathrm{stop}}$ experiments (Polymeris et al. [7]).

It is noted that in the graph in Fig.14, the KP-TL equation fails to describe the TL glow curve very well at lower temperatures. This is due to the approximations made during derivation of the KP-TL equation (Kitis and Pagonis [43]).

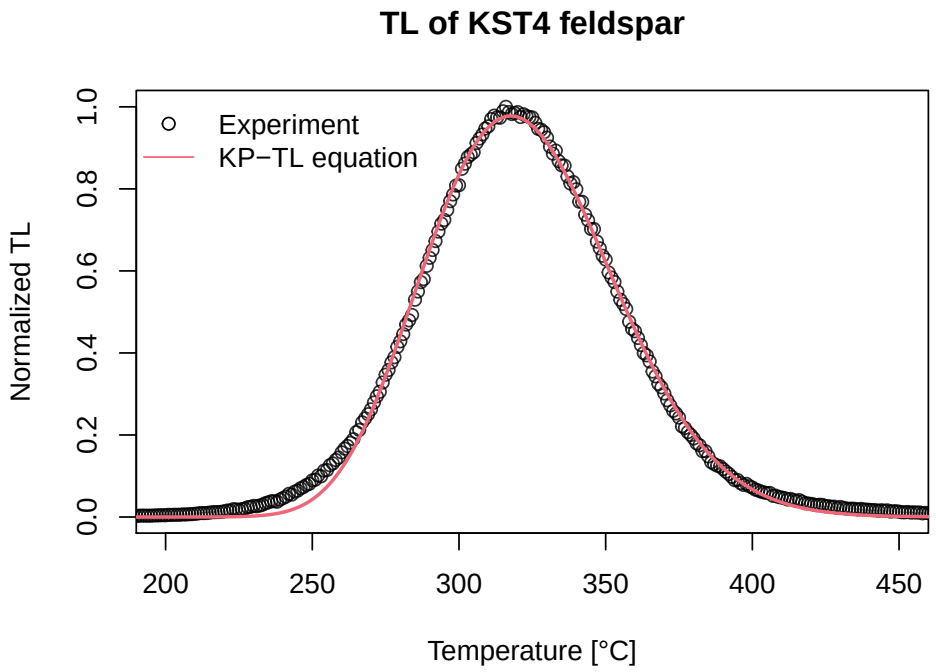

Figure 14: Experimental TL glow curves from freshly irradiated KST4 feldspar sample, fitted using the Kitis-Pagonis analytical Eq.(46). Note that the solid line does not describe the experimental data very accurately at low temperatures, due to the approximations involved in the KP-TL equations. For more details, see Pagonis et al. [33].

13. Discussion and conclusions

In this paper, several compact R functions have been presented, which can be used to simulate the TL and CW-IRSL signals from feldspars. These signals are of a complex nature, however, it is possible to simulate sequences of irradiation and thermal/optical treatments of feldspars in the laboratory, as well as under different thermal conditions in nature.

The key concept that allows this uniform description of luminescence signals from both freshly irradiated as well as pretreated samples, is the time evolution of the nearest neighbor distribution following various optical and thermal events.

The FSF are simple to use and very fast, with running times of all scripts in this paper of the order of seconds. They are also very flexible, the users can immediately change the parameters in the code, and can simulate various behaviors, without the need to carry out numerical integrations, which may become numerically unstable. The accuracy of the FSF was tested against the more accurate numerical integration methods, and the two methods agreed to better than 1%.

All FSF and the four models summarized in this paper are based on first order kinetics, for both irradiation and optical/thermal excitation of the samples. It must also be mentioned that other kinetic models were used previously to simulate the luminescence behavior of feldspars, such as general order kinetics (GOK) models (Biswas et al. [46], Biswas et al. [47], Guralnik et al. [48]). The GOK approach usually fits experimental data on radiation-induced signal growth and isothermal signal decay very well and over a wide parameter space [48], and captures departure from first order behavior of the system. Data from Biswas et al. ([46], [47]) indicate that the trap filling follows first order kinetics in many cases, while the thermal eviction of trapped charge relates to a kinetic order in between 1 and 2.

The approach used in this paper can not be applied to these GOK models, since analytical equations are not available for $n(r', t)$ in the empirically based GOK models.

The FSF presented here can act as a valuable educational tool, but they can also be used as a first step in more complex simulations and research work. As a first example, the FSF can be very useful in improving our understanding of the complex luminescence processes involved during application of the Single Aliquot Regenerative (SAR) protocols applied to feldspars (Wallinga et al. [49], Kars et al. [50]). These protocols involve several stages of irradiation, heating and infrared stimulation of the samples. These stages can be simulated easily using the FSF, by calling sequentially the corresponding R functions. These types of simulations will help researchers understand, for example, the sensitivity changes taking place while applying the SAR protocols in feldspars, and hence may lead to improvements of the relevant experimental protocols.

The system behavior as revealed by the nearest neighbor distribution can be closely tracked throughout the SAR stages and critical steps (e.g., those inducing systematic deviations in dating procedures) be isolated (see for example Friedrich et al. [6], for comparable applications of comprehensive quartz models).

As a second example of possible applications for the FSF, we discuss the important research area of thermochronometry (Herman et al. [51], Li and Li [52], King et al. [28]). As a specific example, the FSF can be applied in a straightforward way to the model developed recently by King et al. [17] for thermochronometry studies of feldspars. The model developed by these authors consists of a combination of first order kinetics equations for irradiation and loss of charge due to tunneling phenomena, but they also incorporated the effect of the band tail states, which are known to play an important role in the luminescence of feldspars. The band-tails are included in the model by King et al. [17] by numerically integrating the first order equations over the extent of the band tail energy distribution (Li and Li [53], Li and Li [18], Jain and Ankjærgaard [19]).

Specifically, in the FOK model of King et al. [17] the concentration of trapped electrons is

described by a function $n\,(r', E_b, t)$ based on three parameters: the elapsed time t,the distance parameter r' and the parameter E_b describing the energy of the band tail states. In principle, it should be a straightforward matter to extend the FSF in this paper to incorporate the band tail states, by adding an integration step over the parameter E_b, as an additional external for-loop in the code. In practice, it will be again easier to replace the integration process with a summation, similar to the ones used in the FSF. Replacement of the integration process with summations is a desirable feature of the R codes, since summations are much faster than formal integration procedures (which can also become occasionally numerically unstable).

Our future plans include the development of such a comprehensive code which takes into account the band-tails, in order to obtain a clearer description of the luminescence processes in feldspars, both in nature and under laboratory conditions.

Acknowledgments

We thank Prof Dr Georgina King for valuable comments and helpful suggestions on an earlier version of this paper.

Sebastian Kreutzer received funding from the European Union's Horizon 2020 research and innovation programme under the Marie Skłodowska-Curie grant agreement No 844457 (project: CREDit).

FIGURE CAPTIONS

Figure 1 (a) A cube with side $d = 100$ nm contains 50 electrons (triangles) and 300 recombination centers (circles). (b) Histogram of the actual nearest neighbor distances (in nm) of electron-acceptor pairs from the cube in (a). The solid line represents the analytical equation for the distribution of nearest neighbors Eq.(4) [16].

Figure 2 Schematic depiction of the four models: (a) The ground state tunneling (GST) model (Tachiya and Mozumder [12], Huntley [21]). (b) The more general irradiation and ground state tunneling (IGST) model, in which anomalous fading and natural irradiation are taking place simultaneously (Huntley and Lian [22]). (c) The excited state tunneling (EST) model (Jain et al. [13]) (d) Simultaneous irradiation and thermally assisted excited state tunneling (TA-EST) model by Brown et al. [9].

Figure 3 Examples of using the FSF *AFfortimeT(),* to evaluate the nearest neighbor distribution at different times $t = 0, 10^2, 10^4, 10^6$ a. The solid line represents the *unfaded* nearly symmetric distribution at time $t = 0$. As the time after irradiation increases, the "tunneling front" is the almost vertical line which moves to the right, as more and more electrons are recombining at larger distances r'.

Figure 4 (a) Simulation of long term anomalous fading in nature over a time period of 10^4 years, starting with an unfaded sample and using the FSF *AFfortimeT()*. The solid line indicates the approximate analytical Eq.(16). (b) Short term AF in the laboratory, over a period of 10 days after the end of irradiation. The parameters in the model are typical for feldspars.

Figure 5 Simulation of irradiation process in nature, using the FSF *irradfortimeT()*. As the irradiation time increases, the asymmetric distribution of distances r' approaches the field saturation distribution ($\times$ symbols). The symmetric curve indicates the initial distribution of distances, for the unfaded sample (o symbols). For additional examples of this type of simulation, see the papers by Li and Li [23], and Kars and Wallinga [25].

Figure 6 Simulation of irradiation process in nature with a slow dose rate of 3 Gy ka^{-1}, using the FSF *irradfortimeT()*. (a) As the irradiation time increases, the asymmetric distribution of distances r' approaches the field saturation distribution. (b) The corresponding dose response curve. For additional examples of dose response curves based on this model, see Li and Li [23], and Kars and Wallinga [25].

Figure 7 Simulation of irradiation process in the *laboratory*, using the FSF *irradfortimeT()*. The dose rate is 0.1 Gy s^{-1} and the irradiation times $t_{irr} = 1 - 10^6$ s. As the irradiation time increases, both the asymmetric distribution of distances r' in (a), and the trap filling ratio $n(t)/N$ in (b) approach saturation.

Figure 8 Simulation of CW-IRSL experiment for freshly irradiated samples, using the three FSF *CWfortimeT()*, *stimIRSL()* and *CWsignal()*. (a) The distributions of distances at the beginning and at the end of the CW-IRSL experiment ; (b) The CW-IRSL curves evaluated for each distance r'; (c) The sum of the curves shown in (b), yields the total CW-IRSL signal. The solid line in (c) is the analytical KP-CW equation developed by Kitis and Pagonis [43] . The parameters in the model are typical for feldspars.

Figure 9 Simulation of TL glow curve for freshly irradiated samples using the FSF *heatTo()*, *stimTL()* and *heatAt()*. The sample is heated up to 400°C, just below the high temperature end of the TL glow curve. (a) The distributions of distances r' before and after the heating the sample are shown as circles and triangles, respectively; (b) The partial first order TL glow curves; (c) The sum of the glow curves from (b).

Figure 10 Several examples of the simulation functions for thermally and optically treated samples, using the FSF. The parameters in the model are typical for feldspars. (1) TL for unfaded sample; (2) Heat to temperature T_{PH}=320°C, then measure TL; (3) Heat for 30 s at T_{PH}=320°C, then measure TL; (4) CW-IRSL excitation for 50 s, then measure TL.

Figure 11 Simulation of irradiations in nature using the FSF *irradandThermalfortimeT()* in the TA-EST model, for a fixed burial temperature of −4°C. (a) The distributions of the distance parameter r' at various irradiation times. Compare the shape of these distributions with Fig.6. (b) The corresponding dose response shown as the trap filling ratio $n(t)/N$.

Figure 12 Multiple irradiations in nature using the FSF *irradatsometemp()* in the TA-EST model, for variable burial temperatures T_{irr}= -4, 0, 4, 8 °C and for a fixed irradiation time $t_{irr} = 10^3$ a.

Figure 13 Experimental CW-IRSL glow curves from freshly irradiated KST4 feldspar sample, fitted using the Kitis-Pagonis analytical Eq.(44). For more details, see Pagonis et al. [33].

Figure 14 Experimental TL glow curves from freshly irradiated KST4 feldspar sample, fitted using the Kitis-Pagonis analytical Eq.(46). Note that the solid line does not describe the experimental data very accurately at low temperatures, due to the approximations involved in the KP-TL equations. For more details, see Pagonis et al. [33].

References

[1] R. Chen, V. Pagonis, Thermally and Optically Stimulated Luminescence: A Simulation Approach, John Wiley & Sons, Chichester, 2011.

[2] E. G. Yukihara, S. W. S. McKeever, Optically stimulated luminescence, Wiley (2011). doi:10.1002/9780470977064.

[3] G. Kitis, G. S. Polymeris, V. Pagonis, Stimulated luminescence emission: From phenomenological models to master analytical equations, Applied Radiation and Isotopes 153 (2019) 108797. doi:https://doi.org/10.1016/j.apradiso.2019.05.041.
URL http://www.sciencedirect.com/science/article/pii/S0969804319304142

[4] R. M. Bailey, Towards a general kinetic model for optically and thermally stimulated luminescence of quartz, Radiation Measurements 33 (1) (2001) 17–45.

[5] V. Pagonis, A. G. Wintle, R. Chen, X. L. Wang, A theoretical model for a new dating protocol for quartz based on thermally transferred OSL (TT-OSL), Radiation Measurements 43 (2008) 704 – 708.

[6] J. Friedrich, S. Kreutzer, C. Schmidt, Solving ordinary differential equations to understand luminescence: 'RLumModel', an advanced research tool for simulating luminescence in quartz using R , Quaternary Geochronology 35 (2016) 88 – 100.

[7] G. S. Polymeris, V. Pagonis, G. Kitis, Thermoluminescence glow curves in preheated feldspar samples: An interpretation based on random defect distributions, Radiation Measurements 97 (2017) 20 – 27. doi:http://dx.doi.org/10.1016/j.radmeas.2016.12.012.
URL http://www.sciencedirect.com/science/article/pii/S1350448716303262

[8] V. Pagonis, N. Brown, G. S. Polymeris, G. Kitis, Comprehensive analysis of thermoluminescence signals in Mg_4BO_7: Dy, Na dosimeter, Journal of Luminescence 213 (2019) 334 – 342. doi:https://doi.org/10.1016/j.jlumin.2019.05.044.
URL http://www.sciencedirect.com/science/article/pii/S0022231319306519

[9] N. D. Brown, E. J. Rhodes, T. M. Harrison, Using thermoluminescence signals from feldspars for low-temperature thermochronology, Quat. Geochronol. 42 (2017) 31–41. doi:10.1016/j.quageo.2017.07.006.

[10] R Core Team, R: A Language and Environment for Statistical Computing, R Foundation for Statistical Computing, Vienna, Austria. https://www.r-project.org (2020).
URL https://www.R-project.org/

[11] V. Pagonis, R. Chen, C. Kulp, G. Kitis, An overview of recent developments in luminescence models with a focus on localized transitions, Radiation Measurements 106 (2017) 3 – 12. doi:https://doi.org/10.1016/j.radmeas.2017.01.001.
URL http://www.sciencedirect.com/science/article/pii/S1350448717300094

[12] M. Tachiya, A. Mozumder, Decay of trapped electrons by tunnelling to scavenger molecules in low-temperature glasses, Chemical Physics Letters 28 (1) (1974) 87 – 89. doi:https://doi.org/10.1016/0009-2614(74)80022-9.
URL http://www.sciencedirect.com/science/article/pii/0009261474800229

[13] M. Jain, B. Guralnik, M. T. Andersen, Stimulated luminescence emission from localized recombination in randomly distributed defects, Journal of Physics: Condensed Matter 24 (38) (2012) 385402.

[14] K Soetaert, plot3D: Plotting multi-dimensional data. R package version 1.3. (2019).
URL https://CRAN.R-project.org/package=plot3D

[15] A Beygelzimer, S Kakadet, J Langford, S Arya, D Mount and S Li , FNN: Fast nearest neighbor search algorithms and applications. R package version 1.1.3. (2019).
URL https://CRAN.R-project.org/package=FNN

[16] V. Pagonis, C. Kulp, Monte Carlo simulations of tunneling phenomena and nearest neighbor hopping mechanism in feldspars, Journal of Luminescence 181 (2017) 114–120.

[17] G. E. King, F. Herman, R. Lambert, P. G. Valla, B. Guralnik, Multi OSL thermochronometry of feldspar, Quaternary Geochronology 33 (2016) 76–87.

[18] B. Li, S.-H. Li, The effect of band-tail states on the thermal stability of the infrared stimulated luminescence from k-feldspar, Journal of Luminescence 136 (2013) 5 – 10. doi:https://doi.org/10.1016/j.jlumin.2012.08.043.
URL http://www.sciencedirect.com/science/article/pii/S0022231312005248

[19] M. Jain, C. Ankjærgaard, Towards a non-fading signal in feldspar: Insight into charge transport and tunnelling from time-resolved optically stimulated luminescence, Radiation Measurements 46 (3) (2011) 292 – 309. doi:http://dx.doi.org/10.1016/j.radmeas.2010.12.004.
URL http://www.sciencedirect.com/science/article/pii/S1350448710004038

[20] N. R. J. Poolton, K. B. Ozanyan, J. Wallinga, A. S. Murray, L. Bøtter-Jensen, Electrons in feldspar II: a consideration of the influence of conduction band-tail states on luminescence processes, Physics and Chemistry of Minerals 29 (3) (2002) 217–225.

[21] D. J. Huntley, An explanation of the power-law decay of luminescence, Journal of Physics: Condensed Matter 18 (4) (2006) 1359.

[22] D. J. Huntley, O. B. Lian, Some observations on tunnelling of trapped electrons in feldspars and their implications for optical dating, Quaternary Science Reviews 25 (19-20) (2006) 2503–2512.

[23] B. Li, S. H. Li, , Journal of Physics D: Applied Physics 41 (22) (2008) 225502. doi:10.1088/0022-3727/41/22/225502.
URL

[24] R. H. Kars, J. Wallinga, K. M. Cohen, A new approach towards anomalous fading correction for feldspar IRSL dating , tests on samples in field saturation, Radiation Measurements 43 (2) (2008) 786 – 790. doi:https://doi.org/10.1016/j.radmeas.2008.01.021.
URL http://www.sciencedirect.com/science/article/pii/S1350448708000401

[25] R. H. Kars, J. Wallinga, IRSL dating of K-feldspars: Modelling natural dose response curves to deal with anomalous fading and trap competition, Radiation Measurements 44 (5) (2009) 594–599.

[26] P. Thioulouse, E. A. Giess, I. F. Chang, Investigation of thermally stimulated luminescence and its description by a tunneling model, Journal of Applied Physics 53 (12) (1982) 9015–9020. arXiv:https://doi.org/10.1063/1.330409, doi:10.1063/1.330409.
URL https://doi.org/10.1063/1.330409

[27] I. F. Chang, P. Thioulouse, Treatment of thermostimulated luminescence, phosphorescence, and photostimulated luminescence with a tunneling theory, Journal of Applied Physics 53 (8) (1982) 5873–5875. arXiv:https://doi.org/10.1063/1.331427, doi:10.1063/1.331427.
URL https://doi.org/10.1063/1.331427

[28] G. E. King, B. Guralnik, P. G. Valla, F. Herman, Trapped-charge thermochronometry and thermometry: A status review, Chemical Geology 44 (2016) 3–17. doi:http://dx.doi.org/10.1016/j.chemgeo.2016.08.023.

[29] V. Pagonis, C. Schmidt, S. Kreutzer, vpagonis/FSF-paper: FSF paper v1.0 (Version V1.0). (2021, January 8). Zenodo. http://doi.org/10.5281/zenodo.4429270 . doi:10.5281/ZENODO.4429270.

[30] M. Lamothe, M. Auclair, C. Hamzaoui, S. Huot, Towards a prediction of long-term anomalous fading of feldspar IRSL, Radiation Measurements 37 (4) (2003) 493–498.

[31] R. Visocekas, Tunnelling in afterglow: its coexistence and interweaving with thermally stimulated luminescence, Radiation Protection Dosimetry 100 (2002) 45–53. doi:10.1093/oxfordjournals.rpd.a005911.

[32] R. Visocekas, V. Tale, A. Zink, I. Tale, Trap spectroscopy and tunnelling luminescence in feldspars, Radiation Measurements 29 (1998) 427–434. doi:10.1016/s1350-4487(98)00062-6.

[33] V. Pagonis, J. Friedrich, M. Discher, A. Müller-Kirschbaum, V. Schlosser, S. Kreutzer, R. Chen, C. Schmidt, Excited state luminescence signals from a random distribution of defects: A new Monte Carlo simulation approach for feldspar, Journal of Luminescence 207 (2019) 266–272. doi:https://doi.org/10.1016/j.jlumin.2018.11.024.
URL http://www.sciencedirect.com/science/article/pii/S0022231318317368

[34] V. Pagonis, G. Kitis, Mathematical aspects of ground state tunneling models in luminescence materials, Journal of Luminescence 168 (2015) 137–144.

[35] V. Pagonis, M. Jain, K. J. Thomsen, A. S. Murray, On the shape of continuous wave infrared stimulated luminescence signals from feldspars: A case study, Journal of Luminescence 153 (2014) 96–103.

[36] I. K. Sfampa, G. S. Polymeris, N. Tsirliganis, V. Pagonis, G. Kitis, Prompt isothermal decay of thermoluminescence in an apatite exhibiting strong anomalous fading, Nuclear Instruments and Methods in Physics Research Section B: Beam Interactions with Materials and Atoms 320 (2014) 57–63. doi:https://doi.org/10.1016/j.nimb.2013.12.003.
URL http://www.sciencedirect.com/science/article/pii/S0168583X13011646

[37] I. K. Sfampa, G. S. Polymeris, V. Pagonis, E. Theodosoglou, N. Tsirliganis, G. Kitis, Correlation of basic TL, OSL and IRSL properties of ten K-feldspar samples of various origins, Nuclear Instruments and Methods in Physics Research Section B: Beam Interactions with Materials and Atoms 359 (2015) 89 – 98. doi:https://doi.org/10.1016/j.nimb.2015.07.106.
URL http://www.sciencedirect.com/science/article/pii/S0168583X15006849

[38] G. Kitis, G. S. Polymeris, E. Sahiner, N. Meric, V. Pagonis, Influence of the infrared stimulation on the optically stimulated luminescence in four K-feldspar samples, Journal of Luminescence 176 (2016) 32 – 39. doi:https://doi.org/10.1016/j.jlumin.2016.02.023.
URL http://www.sciencedirect.com/science/article/pii/S0022231315305846

[39] E. Şahiner, G. Kitis, V. Pagonis, N. Meriç, G. S. Polymeris, Tunnelling recombination in conventional, post-infrared and post-infrared multi-elevated temperature IRSL signals in microcline K-feldspar, Journal of Luminescence 188 (2017) 514–523.

[40] V. Pagonis, C. Kulp, C. Chaney, M. Tachiya, Quantum tunneling recombination in a system of randomly distributed trapped electrons and positive ions., Journal of Physics. Condensed matter 29 (2017) 365701. doi:10.1088/1361-648X/aa7db5.

[41] N. R. J. Poolton, J. Wallinga, A. S. Murray, E. Bulur, L. Bøtter-Jensen, Electrons in feldspar I: on the wavefunction of electrons trapped at simple lattice defects, Physics and Chemistry of Minerals 29 (3) (2002) 210–216.
URL https://doi.org/10.1007/s00269-001-0217-3

[42] M. Jain, R. Sohbati, B. Guralnik, A. S. Murray, M. Kook, T. Lapp, A. K. Prasad, K. J. Thomsen, J. P. Buylaert, Kinetics of infrared stimulated luminescence from feldspars, Radiation Measurements 81 (2015) 242 – 250. doi:http://dx.doi.org/10.1016/j.radmeas.2015.02.006.
URL http://www.sciencedirect.com/science/article/pii/S1350448715000335

[43] G. Kitis, V. Pagonis, Analytical solutions for stimulated luminescence emission from tunneling recombination in random distributions of defects, Journal of Luminescence 137 (2013) 109–115. doi:https://doi.org/10.1016/j.jlumin.2012.12.042.
URL http://www.sciencedirect.com/science/article/pii/S0022231312007624

[44] V. Pagonis, N. Brown, On the unchanging shape of thermoluminescence peaks in preheated feldspars: Implications for temperature sensing and thermochronometry, Radiation Measurements 124 (2019) 19–28.

[45] N. D. Brown, E. J. Rhodes, Thermoluminescence measurements of trap depth in alkali feldspars extracted from bedrock samples, Radiation Measurements 96 (2017) 53–61. doi:10.1016/j.radmeas.2016.11.011.

[46] R. H. Biswas, F. Herman, G. E. King, J. Braun, Thermoluminescence of feldspar as a multi-thermochronometer to constrain the temporal variation of rock exhuma-

tion in the recent past, Earth and Planetary Science Letters 495 (2018) 56–68. doi:10.1016/j.epsl.2018.04.030.

[47] R. H. Biswas, F. Herman, G. E. King, B. Lehmann, A. K. Singhvi, Surface paleothermometry using low-temperature thermoluminescence of feldspar, Climate of the Past 16 (6) (2020) 2075–2093. doi:10.5194/cp-16-2075-2020.
URL https://cp.copernicus.org/articles/16/2075/2020/

[48] B. Guralnik, B. Li, M. Jain, R. Chen, R. B. Paris, A. S. Murray, S. Li, V. Pagonis, P. G. Valla, F. Herman, Radiation-induced growth and isothermal decay of infrared-stimulated luminescence from feldspar, Radiation Measurements 81 (2015) 224 – 231. doi:http://dx.doi.org/10.1016/j.radmeas.2015.02.011.
URL http://www.sciencedirect.com/science/article/pii/S1350448715000384

[49] J. Wallinga, A. Murray, A. Wintle, The single-aliquot regenerative-dose (SAR) protocol applied to coarse-grain feldspar, Radiation Measurements 32 (5) (2000) 529 – 533. doi:https://doi.org/10.1016/S1350-4487(00)00091-3.
URL http://www.sciencedirect.com/science/article/pii/S1350448700000913

[50] R. H. Kars, T. Reimann, J. Wallinga, Are feldspar SAR protocols appropriate for post-IR IRSL dating?, Quaternary Geochronology 22 (2014) 126 – 136. doi:https://doi.org/10.1016/j.quageo.2014.04.001.
URL http://www.sciencedirect.com/science/article/pii/S1871101414000326

[51] F. Herman, E. J. Rhodes, J. Braun, L. Heiniger, Uniform erosion rates and relief amplitude during glacial cycles in the Southern Alps of New Zealand, as revealed from OSL-thermochronology, Earth and Planetary Science Letters 297 (1) (2010) 183 – 189. doi:https://doi.org/10.1016/j.epsl.2010.06.019.
URL http://www.sciencedirect.com/science/article/pii/S0012821X10003936

[52] B. Li, S.-H. Li, Determining the cooling age using luminescence-thermochronology, Tectonophysics 580 (2012) 242 – 248. doi:http://dx.doi.org/10.1016/j.tecto.2012.09.023.
URL http://www.sciencedirect.com/science/article/pii/S0040195112006002

[53] B. Li, S. H. Li, Thermal stability of infrared stimulated luminescence of sedimentary K-feldspar, Radiation Measurements 46 (1) (2011) 29 – 36. doi:http://dx.doi.org/10.1016/j.radmeas.2010.10.002.
URL http://www.sciencedirect.com/science/article/pii/S1350448710003495